

This is a non-peer-reviewed preprint submitted to EarthArXiv.

This manuscript has been submitted for publication in *Frontiers in Environmental Science*. Please note the manuscript has yet to be formally accepted for publication. Subsequent versions of this manuscript may have slightly different content. If accepted, the final version of this manuscript will be available via the 'Peer-reviewed Publication DOI' link on the right-hand side of this webpage. Please feel free to contact any of the authors; we welcome feedback.

Long-term trends and drivers of water color in Missouri reservoirs

- 2 Lorena Pinheiro-Silva^{1,2*}, Greg M. Silsbe¹, David C. Richardson^{2,3}, Rebecca L. North²
- ¹Horn Point Laboratory, University of Maryland Center for Environmental Science, Cambridge, Maryland,
- 4 USA.

- ²School of Natural Resources, University of Missouri-Columbia, Columbia, Missouri, USA.
- 6 ³State University of New York at New Paltz, New Paltz, New York, USA.
- 7 * Corresponding author: lsilva@umces.edu
- 8 **Keywords:** Midwest, man-made systems, dominant wavelength, water quality, satellite remote sensing.

9 Abstract

10

11 12

13

14

15

16

17

18 19

20

21

22

23 24

25

26 27

28

29

Contrasting water quality trends are occurring within and across North America, with waterbodies experiencing increasing phytoplankton blooms, increasing dissolved organic matter, or both, while others are becoming clearer and bluer; dramatically changing water color. To assess the spatial and temporal variability in water color, we quantified trends in satellite-derived dominant wavelength (λ_d) from 1984 to 2020 for 484 reservoirs in Missouri reservoirs using the LimnoSat-US dataset. Currently, the vast majority of Missouri reservoirs are classified as green and within a range (538–555 nm) that lies closer to the brown, rather than blue, color endmember. Nearly one-third of reservoirs (n = 159) experienced significant temporal shifts in water color, with more (n = 91) negative (e.g., bluer) than positive $(n = 68) \lambda_d$ trends. Linear mixed-effect models indicate that periods of extreme wetness and drought are associated with browner and bluer waters, respectively, and boosted regression trees further reveal that waterbody and watershed characteristics are important predictors for water color trends. We also analyzed trends in summer water quality (WQ) parameters from two long-term monitoring programs to evaluate independent and synchronous changes with λ_d . We provide analyses showing that particulate inorganic matter and Secchi depth most strongly correlated with λ_d , and surprisingly total nitrogen and total phosphorus concentrations that are not typically associated with satellite-derived data have greater co-variance with λ_d than chlorophyll a. We further demonstrate that while λ_d trends broadly aligns with changes in water quality, co-occurring water quality and color trends in Missouri reservoirs at times defy a simplistic canonical interpretation, particularly in eutrophic water bodies where changes in nutrient concentration, chlorophyll a and water color can occur independent of each other. Our results help explain some of the previously observed heterogeneous controls on water color and emphasize the importance of integrating water quality data alongside commonly used landscape and morphological features.

1. Introduction

Contrasting water quality trends are occurring within and across North America, with waterbodies experiencing oligotrophication (aka 'blueing'; Sillen et al., 2024), eutrophication (aka 'greening'; Schindler et al., 2012), brownification (aka 'browning'; Monteith et al., 2007; Roulet and Moore, 2006), or both simultaneously (aka "murky" lakes; Leech et al., 2018). Water color, as perceived by the human eye, is one of the oldest indicators of water quality parameters and is closely linked to productivity and trophic state of aquatic ecosystems (Topp et al., 2021). A number of commonly measured water quality variables can be estimated directly from direct or remotely-sensed measures of color including chlorophyll a (chl a; Smith et al., 2020), total suspended solids (TSS; Ondrusek et al., 2012), and colored dissolved organic matter (CDOM; Cao et al., 2018). Indeed much of our understanding of canonical shifts in water quality are intertwined with changes in color. For instance, high nutrient loads into waterbodies from urban, agricultural, and industrial sources result in increased chl a (proxy for phytoplankton productivity) and greener waters (Dodds et al., 2009). Increases in CDOM due to changes in climate, hydrology, land cover, and atmospheric deposition (Erlandsson et al., 2008; Freeman et al., 2001; Monteith et al., 2007) have led to brown waters (Leech et al., 2018). Conversely, factors such as lake acidification (Charifson et al., 2015), low precipitation (Hongve et al., 2004), increased rates of filter-feeding by zebra mussels (Binding et al., 2007), or reductions in nutrient loading (Jeppesen et al., 2005) lead to increased water transparency and bluer waters. The nutrient-color paradigm (Williamson et al., 1999) conceptualizes the interaction between total phosphorus (TP) and CDOM in lakes where blue waters are oligotrophic (low TP and CDOM), green waters are eutrophic (high TP, low CDOM), and brown waters are either dystrophic (low TP, high CDOM) or mixotrophic ('murky', high TP and CDOM; Oleksy et al., 2024; Williamson et al., 1999).

Water color's strong representativeness and accessibility through remote sensing make it an attractive indicator for monitoring changes in the ecological state and environmental conditions of aquatic ecosystems (Shen et al., 2025). Satellite-based monitoring offers a cost-effective alternative, providing broad spatial and temporal coverage, but its application to inland waters has been hindered by the limited capabilities of satellite sensors not specifically designed for coastal and inland waters applications and by challenges such as atmospheric correction, land adjacency, and bottom reflectance (Mouw et al., 2015). Recent advances, including improved atmospheric correction algorithms (Castagna and Vanhellemont, 2025), machine learning approaches (Smith et al., 2020), and robust analysis-ready databases (King et al., 2024; Topp et al., 2020), collectively aim to improve data quality and accessibility. Satellite-derived dominant wavelength (λ_d) has emerged as a widely used descriptor because it captures the perceived hue of water, is readily derived from virtually all earth observing satellites, and provides a consistent metric for studying long-term water quality changes at broad scales (Gardner et al., 2021; Yang et al., 2022). Studies using λ_d have revealed the importance of climate, landscape characteristics and waterbody morphology in driving water color trends (Cao et al., 2023; Liu et al., 2024; Oleksy et al., 2022; Shen et al., 2025).

Despite large scale studies efforts (Gardner et al., 2021; Yang et al., 2022), the factors driving changes in water quality and color may differ both among individual waterbodies and across geographic regions (Cao et al., 2023a). As a result, more focused regional scale studies may be more effective for describing parallel changes in water quality and water color. However, the scarcity of long-term *in-situ* data has limited our ability to assess these dynamics over broad spatial and temporal scales. This study integrates 37 years of satellite-derived water color observations from the analysis-ready LimnoSat dataset with detailed field-based measurements from long-term water quality monitoring programs in the state of Missouri to (1) quantify secular and synchronous changes in summer water color and water quality in Missouri reservoirs over the past several decades and (2) identify climate, landscape characteristics, and waterbody morphology factors driving the

spatial and temporal trends. Inspired by the nutrient-color paradigm, this study examines covariation in not just optically active parameters and water color (e.g. Chl a, TSS) but also tests the suitability of λ_d as a predictor of changes in total phosphorus (TP) and total nitrogen (TN) through time. By compiling a uniform dataset from open data repositories and statewide long-term water quality programs, our study not only aims to unravel the key drivers of regional trends in water color and quality in the study region, but also demonstrates the potential for integrating satellite-based measurements with traditional monitoring to strengthen future research; particularly in times of reduced funding for environmental monitoring programs.

2 Material and Methods

2.1 Study Area and Geospatial Analysis

Most of Missouri's (MO) waterbodies are human-constructed reservoirs embedded across the state's six Environmental Protection Agency (EPA) ecoregions (Ozark Highlands, Central Irregular Plains, Western Corn Belt Plains, Interior River Valleys and Hills, the Mississippi Alluvial Plain, and Mississippi Valley Loess Plains; Figure 1A). Geospatial data for individual reservoirs, published by the MO Department of Natural Resources (MDNR) was separately matched in space with the *in situ* water quality monitoring datasets and the remote sensing dataset described below. The MDNR identifies a total of 2,547 reservoirs, of which 484 have remotely sensed data with \geq 20 consecutive years of summer color observations (Section 2.2); 298 have water quality data (Section 2.3), and 160 have co-located water quality and remotely sensed time series (Figure 1A).

Watersheds were delineated using the Python package PySheds and USGS 60 m digital elevation data. Watershed land cover was extracted from the 2021 release of the National Land Cover Database (NLCD), developed primarily by the U.S. Geological Survey (USGS) in collaboration with the Multi-Resolution Land Characteristics (MRLC) Consortium. Geomorphological data, specifically elevation, area, perimeter, and elongation ratios were derived for each reservoir and watershed. The elongation ratio is defined as the ratio of the diameter of a circle with an equivalent area to that of the reservoir/watershed to its maximum length (i.e., the maximum distance between all coordinate pairs along the perimeter; Sukristiyanti et al., 2018). High elongation ratios therefore represent more circular reservoirs/watersheds and generally coincide with flat land and low relief. Smaller elongation ratios correspond to more narrow and dendritic reservoirs/watersheds with high relief and steep slopes (Sukristiyanti et al., 2018). All geospatial analysis was performed in Python, and the functions and libraries used for each calculation are listed (Table S1).

Hydrometeorological variations in space and time were analyzed using the Palmer drought severity index (PDSI). The PDSI index quantifies the severity of wet and dry conditions by using estimates of relative soil moisture conditions based on temperature, precipitation, and evapotranspiration anomalies. PDSI values less than -3 indicate severe drought conditions, and PDSI values greater than 3 indicate very moist conditions. PDSI for summers from 1990 to 2020 were obtained from the daily high-spatial resolution Gridded Surface Meteorological (gridMET) dataset available on the Google Earth Engine (GEE) platform.

2.2 Water Color

Remotely-sensed reflectance data and the resultant visible dominant wavelength (λ_d) were obtained for 484 waterbodies in Missouri from the LimnoSat-US database (Topp et al., 2020). The main criterion for selecting the studied reservoirs was the availability of 20 consecutive years of data between 1984 and 2020. For inland waterbodies in the U.S. larger than 0.1 km², LimnoSat contains all cloud-free Landsat (5, 7, and 8) surface reflectance (T1-SR) data where for each waterbody and timestamp, the median reflectance is derived

from pixels within 120 m of the Chebyshev Center (i.e., the deepest point that is furthest away from the shoreline). Landsat 5 and 7 imagery have been atmospherically corrected using the Landsat Ecosystem Disturbance Adaptive Processing System (LEDAPS), while Landsat 8 imagery has been corrected using the Landsat Surface Reflectance Code (LaSRC). Bands for each sensor were standardized across time and between satellites (Topp et al., 2021), ensuring the reliability of long-term trend analyses (Shen et al., 2025). Dominant wavelength is calculated by converting surface reflectance values into the chromaticity color space, following Wang et al. (2015). For each reservoir and year, the mean λ_d was computed across the stratified season (May 1 to Oct 31) to align with the water quality sampling period.

A variety of λ_d thresholds have been used in the literature to delineate blue from green waterbodies and green from brown waterbodies. In the Missouri LimnoSat data blue reflectance is maximal where $\lambda_d \leq 495$ nm (blue reservoirs), red reflectance is maximal where $\lambda_d \geq 575$ nm (brown reservoirs), such that green reservoirs have λ_d between 495 nm < λ_d < 575 nm (Figure S1). Within the green spectral range, blue reflectance steadily declines while red reflectance steadily increases (Figure S1), such that decreasing trends in λ_d can be described as blueing and increasing trends in λ_d can be described as browning.

2.3 In situ Water Quality Dataset

114115

116 117

118 119

120

121

122123

124

125

126

127

128

129 130

131

132 133

134 135

136 137

138

139 140

141

142

143

144

145

146

147

148

149

150

151

152

153 154

Water quality parameters for 298 waterbodies in Missouri from 1984 to 2020 were obtained through the Statewide Lake Assessment Program (SLAP) and the community science led Lakes of Missouri Volunteer Program (LMVP), aligning with the LimnoSat-US data availability. In each waterbody, surface water quality samples are collected alongside vertical profiles on 3 or 4 occasions between May and October each year, in close proximity to the deepest part of the reservoir (i.e., near-dam locations). Water temperature and dissolved oxygen profiles, recorded in meter increments (1984 - 2016) or continuous profiles (2017 - 2020) from the surface to the bottom, were obtained using multiple YSI sondes over the years (see Table S2). These data were used to calculate average water temperature and dissolved oxygen concentrations in the epilimnion (above the top of the metalimnion) and the hypolimnion (below the bottom of the metalimnion). The thermal stability index, Brunt-Väisälä buoyancy frequency (N2; s-2), was calculated based on the density gradient of the water column in the R statistical environment, version 4.4.2 (The R Development Core Team 2024; Table S1). Thermocline depth at 0.3 kg m⁻³/m density threshold was derived from water temperature profiles. Water transparency (Secchi) was assessed using a Secchi disk. Surface water samples refer to either samples from 0.5 m depth or epilimnetic integrated samples (Figure S2). Water samples were stored in high density polyethylene (HDPE) bottles, placed into coolers, and frozen until analysis. After freezing, they were analyzed by standard methods (Table S2) for particulate organic matter (POM; mg/L), particulate inorganic matter (PIM; mg/L), total suspended solids (TSS; mg/L), total phosphorus (TP; µmol/L), total nitrogen (TN; µmol/L), uncorrected chlorophyll a (Chl a; µg/L), and dissolved organic carbon (DOC; µmol/L). Sampling and analytical methodology were consistent throughout, except for chl a, TP, and TN (Table S2). We also determined the ratios of TN and TP (TN/TP), POM and TSS (POM/TSS), PIM and TSS (PIM/TSS).

2.4 Data Analysis

2.4.1 Trend Analysis

All water quality and λ_d trend analyses were performed on reservoir specific annual data averaged across the thermally stratified season (May 1 to Oct 31). Rates of change were estimated using Sen's slope (Q; see Table S3 for statistical references), and the statistical significance of resultant trends was assessed using the non-parametric Mann-Kendall trend test (MK; Table S3). Secular trends of λ_d (i.e. $\Delta\lambda_d$) are limited to reservoirs

with a minimum of 20 consecutive years of data between 1984 and 2020 (n = 484, Figure S3). Missing values inside the time series were imputed using linear interpolation, allowing a maximum gap of two consecutive missing years. To assess differences in the most recent λ_d and $\Delta\lambda_d$ across ecoregions and watershed land cover types, we used nonparametric Kruskal-Wallis tests. When significant differences were found, pairwise Dunn's post-hoc tests with Bonferroni-adjusted p-values were applied to identify specific group differences.

Secular trends of water quality parameters were derived as above but restricted to reservoirs with at least 10 consecutive years of data between 1984 and 2020 (Figure 2). Not all reservoirs (n = 298) have the required time series available for every variable (Figure S3). To better capture the complexity of water quality dynamics in Missouri reservoirs, two additional analyses were performed. First, linear regression of resultant water quality slopes, regardless of significance, was conducted in pairwise fashion using parameters with >100 co-occurring time series (TP, TN, Chl a, TSS, PIM, POM, Secchi disk). Second, a frequency analysis is presented that counts how often significant water quality trends co-occur within a reservoir, including cases of contrasting trends (e.g., increasing TN and decreasing TP).

2.4.2 Remotely Sensed and In Situ Water Quality Matchup Analysis

To evaluate how well remotely-sensed water color serves as a proxy for water quality and trends, two analyses are performed using a subset of water quality variables that serve as trophic status indicators (Chl a, TN, TP, TSS, POM, PIM, Secchi, DOC). First, λ_d is compared to collocated water quality observation using a 1-day time window from satellite overpass. The final dataset consists 1704 λ_d and near-concurrent in situ water quality parameters across multiple reservoirs. Pairwise Spearman rank correlations was used to evaluate associations between λ_d values and water quality parameters. To assess differences across wavelengths, water quality data were grouped by λ_d values binned at 10-nm and tested for statistically significant differences using nonparametric Kruskal-Wallis tests. When significant differences are detected, pairwise Dunn's post-hoc tests with Bonferroni-adjusted p-values are applied. Second, parallel trends in λ_d and water quality variables are examined in a subset of reservoirs (n = 22) with significant λ_d trends and sufficiently long (≥ 10 years) coincidental water quality data. To assess the degree of correspondence between changes in λ_d and water quality across reservoirs and water quality variables, a simple alignment score was developed as follows. For each reservoir and water quality parameter, a score of +2 is assigned when both trends are statistically significant and in the same direction (e.g., decreasing λ_d and decreasing TP). A score of +1 is assigned when the water quality trend is non-significant but in the same direction as $\Delta \lambda_d$. Scores of -1 and -2 are assigned when water quality are in the opposite direction of $\Delta \lambda_d$ (e.g. decreasing λ_d and increasing TP) and are not significant and significant respectively. Resultant scores were summed across reservoirs and variables and normalized to a scale of -1 to 1.

2.4.3 Boosted Regression Trees

To quantify the relative contributions of geomorphological (waterbody elevation, waterbody and watershed area, waterbody and watershed elongation ratio, Warea/Rarea) and land cover (percent cover of urban, forest, and agriculture lands in the watershed) factors to the dominant wavelength slope ($\Delta\lambda_d$), we employed Boosted Regression Trees (BRTs). Our final dataset included 160 reservoirs with co-located LimnoSat, geomorphological and land cover data, sampled between 1984 and 2020 (Figure 2). The BRT method is a machine learning technique that combines regression decision trees and a boosting algorithm (Elith et al., 2008). At each step, a new tree that best reduces the loss function is fitted to the residuals without changing the existing trees as the model is enlarged (i.e., stagewise). This approach eliminates the need for prior data transformation or outlier elimination, fits complex nonlinear relationships between explanatory and response variables, handles interaction effects between predictors, and accommodates both categorical and

numeric variables, as well as missing data (Elith et al., 2008). BRTs were implemented in the R statistical environment, version 4.4.2 (The R Development Core Team 2024) using the *gbm.step* function, which incorporates cross-validation to identify the optimal number of trees and implements the procedures described by Elith et al. (2008). The functions and libraries used are listed in the Supplementary Material (Table S1).

In BRT modelling, three hyperparameters need to be defined and tuned: The learning rate (lr), which determines the contribution of each tree to the final fitted model; tree complexity (tc), which controls the size of trees and whether interactions between variables should be considered; bag fraction (bf), which specifies the proportion of data, without replacement, from the full training set to be selected at each step. The number of trees (nt) is determined from the combination of lr and tc and, in practice, smaller learning rates and larger tree complexities increase the number of trees. To select the appropriate structure of the BRTs, we fitted 30 combinations with varying values for lr (0.05, 0.01, 0.005, 0.001, 0.0005), tc (1, 5, 10) and bf (0.5, 0.75). Model potential for overfitting and performance was assessed using an 80:20 train:test data split with a 10-fold cross-validation method. First, models with the lowest prediction deviation (i.e., deviance between observed values from the training set and predicted values from the test set) were selected. Then, the performance of these models was further evaluated using three metrics: mean absolute error (MAE; Equation 1), root mean square difference (RMSE; Equation 2), and coefficient of determination (R^2 ; Equation 3). Final model selection was based on the combination of lowest MAE and RMSE and highest R^2 value (i.e., higher R^2 reflects better predictive performance). The metrics were calculated as follows:

$$MAE = \frac{1}{n} \sum_{i=1}^{n} |P_i - O_i| \tag{1}$$

$$RMSE = \sqrt{\frac{1}{n} \sum_{i=1}^{n} (P_i - O_i)^2}$$
 (2)

$$R^{2} = \frac{\sum_{i=1}^{n} (P_{i} - \bar{O})^{2}}{\sum_{i=1}^{n} (O_{i} - \bar{O})^{2}}$$
(3)

Where n is the number of observations, P_i and O_i are the predicted and observed values at i, respectively, and \bar{O} is the mean of the observed data. MAE indicates how close the prediction is to the observed values, while RMSE represents the standard deviation of the residuals. R^2 represents the predictive accuracy of models; it approaches 1 when prediction becomes optimal. The final optimal values of lr, tc, and bf were set to 0.0005, 10, and 0.75, respectively, with a maximum number of trees = 3,100 and a Gaussian error distribution (Table S4).

The selected model was used to calculate the mean relative importance (RI) and cumulative contribution of each predictor in explaining the variability of $\Delta\lambda_d$. The RI is quantified by analyzing the number of times a predictor is selected for splits in regression trees and the improvement it brings to the model's predictive accuracy. The RI of each variable is given by dividing its importance by the sum of importance values across all explanatory variables, collectively summing to 100% (Elith et al., 2008). Higher RI values indicate a stronger influence on the response variable. The cumulative contribution reflects the combined effect of multiple predictors in explaining $\Delta\lambda_d$. It is calculated by ranking predictors in descending order of their mean RI and computing their cumulative contributions as a percentage of the total importance. Significant predictors based on permutation tests of variable importance were used to calculate Shapley values, which quantify how each predictor contributes to predictions across all observations. Finally, SHAP-based dependence plots were then used to interpret and visualize how each predictor's contribution varies across its observed range. Positive SHAP values indicate a contribution to increasing $\Delta\lambda_d$, while negative values indicate a contribution to

decreasing $\Delta \lambda_d$ across the study reservoirs. The functions and libraries used are listed in the Supplementary Material (Table S1).

2.4.5 Linear Mixed-Effect Models

To quantify the influence of hydroclimate (e.g., drought and wetter climate) on water color (λ_d) , we employed linear mixed-effect models (LMMs; Figure 2; see Table S3 for statistical references). In all models, λ_d was the response variable, with reservoir identity included as a random intercept to account for inter-reservoir variability in water color. Fixed effects included PDSI, ecoregion, and their interaction. The inclusion of the interaction term allows us to account for climatic effects that might differ by ecoregion. To capture possible underlying temporal trends in λ_d across reservoirs, year was included as a numeric covariate. The variance explained by LMMs was based on marginal and conditional adjusted R^2 (Nakagawa and Schielzeth, 2013). Marginal adjusted R^2 (R^2m) represents the variance explained by a fixed term, and conditional R^2 (R^2c) represents the variance explained by both fixed and random terms. A visual examination of diagnostic plots was applied to determine the model's goodness of fit. p-values and 95% confidence intervals were calculated using Wald t-tests with Satterthwaite's approximation of degrees of freedom. All models were implemented in the R statistical environment, version 4.4.2 (The R Development Core Team 2024). The functions and libraries used are listed in the Supplementary Material (Table S1).

3 Results

3.1 The Color and Trends in Missouri Reservoirs

The vast majority of Missouri reservoirs are green (n = 458, 94%), and brown reservoirs ($\lambda_d > 575$ nm, n = 24, 5%) are less rare than blue reservoirs ($\lambda_d < 495$ nm, n = 3, 1%). Reservoir color varies by ecoregion and land use (Figure 3). Reservoirs in the largely forested Ozark Highlands have λ_d values that are bluer than all other ecoregions (Kruskal-Wallis; H = 72.58, p < 0.01; Figure 3B), and reservoirs dominated by agriculture and wetland watersheds have λ_d values that are browner than reservoirs in forested, mixed, and urban watersheds (Kruskal-Wallis; H = 94.03, p < 0.01; Figure 3D). Nearly one third (n = 159) of Missouri reservoirs have had statistically significant shifts in reservoir color ($\Delta \lambda_d$, MK analysis, p < 0.05). Amongst these reservoirs, negative $\Delta \lambda_d$ (i.e. bluer) trends are approximately 15% (n = 91) more common than positive $\Delta \lambda_d$ trends (i.e. browner; Table 1). The number of reservoirs that are now bluer exceeded those that are now browner in three of Missouri's six ecoregions (Table 1), however $\Delta \lambda_d$ did not co-vary with ecoregion (Kruskal-Wallis; H = 2.49, p = 0.65; Figure 3C) or land use type (Kruskal-Wallis; H = 8.79, p = 0.07; Figure 3D).

Significant shifts in reservoir color, regardless of direction, are almost exclusively confined to shifts within the green spectrum (Figure 4A). Only 6% of reservoirs (n=10) crossed the 575 nm brown/green threshold, and a single reservoir crossed the 495 nm green/blue threshold. The distribution of all λ_d measurements through time shows that most green reservoirs are closer to the brown rather than blue color threshold (Figure 4B). Across all reservoirs with significant negative (Figure 4C) and positive (Figure 4D) $\Delta\lambda_d$ trends, the majority of both time series begin and end above 540 nm. Amongst reservoirs trending bluer, the period between the Great Mississippi and Missouri Rivers Flood of 1993 and 2008 constitute the greatest period of change, and more recently λ_d has remained fairly constant with the exception of wet years when these reservoirs shift back towards browner water (Figure 4A). Amongst reservoirs trending browner, average shifts in water color through time have been comparatively more gradual.

3.2 Drivers of Reservoir Color Change

To quantify potential drivers in water color ($\Delta\lambda_d$), a Boosted Regression Tree (BRT) analysis was performed with a selection of geomorphological (waterbody elevation, waterbody and watershed area, waterbody and watershed elongation ratio, Warea/Rarea) and land cover (percent cover of urban, forest, and agriculture lands in the watershed) predictors, consistent with previous studies (Cao et al., 2023; Liu et al., 2024; Oleksy et al., 2022; Shen et al., 2025). The final BRT model achieved a MAE of 0.24, a RMSE of 0.32, and an R^2 of 49.9% on independent test data. Overall, waterbody elevation ranked as the most important predictor (RI = 24.71%), followed by urban land cover (RI = 20.33%) and waterbody elongation ratio (RI = 16.34%). The Shapley-derived partial dependence plots for individual predictors (Figure 5) indicate that Missouri reservoirs with increasing λ_d (i.e., browner) are typically located at lower elevations and in areas with a lower percentage of urban land cover (Figure 5A–B). Conversely, reservoirs with decreasing λ_d (i.e., bluer) are found at higher elevations and span a wide range of urban land cover percentages (Figure 5A–B). Morphologically, reservoirs trending browner are generally more elongated, while reservoirs trending bluer are more circular in shape (Figure 5C).

Regardless of overall trends, interannual variations in water color are readily observable across many reservoirs. Averaging across all reservoirs, λ_d varied between 538-555 nm through time, where periods of extreme drought and extreme wetness correspond with bluer and browner waters, respectively (Figure 4A). To further explore the interaction between water color and hydroclimate, a linear mixed-effect model including PDSI, ecoregion, their interaction, and year was constructed. Reservoir identity alone (i.e. mean λ_d) accounts for approximately 38% of the explained variance (Table 2). A further 18% of variance is explained by PDSI, ecoregion and their interaction such that the final model accounts for more than half of the total λ_d variance across the Missouri LimnoSat record ($R^2c = 0.56$; Table 2). PDSI had significant positive effects on λ_d in Central Irregular Plains, Interior River Valleys and Hills, Ozark Highlands, and Western Corn Belt Plains (Table 3). The strongest positive association was observed in the agriculture dominated Central Irregular Plains (slope = 1.07, CI = 0.89 – 1.25). In contrast, in the Ozark Highlands (slope = 0.19, CI = -0.07 – 0.45) changes in PDSI were associated with less pronounced variations in λ_d . The only and strongest negative association was observed in the Mississippi Alluvial Plain (slope = -2.97, CI = -9.05 – 3.12).

3.3 Long-Term Trends in Water Quality Parameters

Averaging across all reservoirs with *in situ* data (minimum of 10 years consecutive data), Chl *a*, POM, and the TN:TP ratio have significantly increased over time (Table 4) alongside numerous physical parameters including surface temperature, thermocline depth and buoyancy frequency (i.e., stratification, Table 4). Conversely, PIM and hypolimnetic temperature and dissolved oxygen have significantly decreased over time (Table 4). All other water quality parameters including TP, TN, Secchi depth, and TSS do not have statistically significant trends. Thus Missouri reservoirs have become warmer and greener (higher Chl *a* and POM, lower PIM) without commensurate trends in water transparency or nutrient concentrations when all *in situ* measurements are averaged across the state.

Analysis of reservoir-specific trends however provides a more granular description of water quality changes. Of the 130 reservoirs with sufficiently long time series, 108 (83%) had a statistically significant trend in at least one of the routinely sampled water quality metrics (TP, TN, Chl a, TSS, POM, PIM, Secchi). Surprisingly single instance trends (i.e., where only a single water quality parameter is changing in a given reservoir) was the most common occurrence (30%), and in these reservoirs Chl a was the most common trend to occur alone (25%) followed by TP (19%). Consistent with statewide trends, Chl a and POM concentrations

have increased in 28% and 33% of monitored reservoirs respectively and decreased in just 5%. PIM has significantly decreased in 24% of reservoirs and increased in 10% of reservoirs (Table 4). TSS, the sum of POM and PIM, has declined (16%) in more reservoirs than where it has increased (11%). Consequently, the water quality indicators with the greatest frequency of significant trends are the POM:TSS and PIM:TSS ratios (Table 4). More than half of all reservoirs have statistically significant trends, with increasing POM:TSS (decreasing PIM:TSS) as the dominant direction (44%, Table 4). With respect to bulk nutrient concentrations, TP has significantly decreased in almost twice as many reservoirs (22%) as it has significantly increased (12%). Moreover, reservoirs with significant decreases in TN and improved water transparency are also both more numerous than reservoirs with significant increases in TN and diminished water transparency (Table 4). Thus, at the reservoir scale, more waterbodies are showing improvements in water clarity and declining nutrient concentrations and more reservoirs have increasing Chl *a* and POM. The most prevalent metric of water quality change is a shift towards a higher fraction of organic matter within the total suspended solids pool.

Pairwise linear regression of reservoir-scale water quality slopes, regardless of significance, was conducted on a subset of variables (TP, TN, Chl a, TSS, PIM, PO, Secchi). All slopes were correlated (p < 0.05) and all regression coefficients were positive (e.g. TN and TP slopes positively co-vary), with the exception of water transparency where unlike the other water quality parameters a positive slope (deeper transparency) reflects an improvement in water quality. Inspection of the pairwise coefficients of determination (Table S5) shows that Chl a trends share the strongest association with POM trends ($R^2 = 0.60$) followed by TN trends ($R^2 = 0.47$). The only other coefficients of determination greater than 0.5 were TN and POM slopes ($R^2 = 0.60$), PIM and TSS slopes ($R^2 = 0.64$), and POM and TSS slopes ($R^2 = 0.58$). Notably, the coefficients of determination between TP and other water quality slopes were small (TN: $R^2 = 0.22$, Chl a: $R^2 = 0.12$, Secchi: $R^2 = 0.05$, Table S5).

A second analysis was conducted to quantify how often significant water quality trends co-occur within reservoirs, and separating these into aligned trends (e.g., increasing TP and TN or decreasing TP and TN) and contrasting trends (e.g., increasing TP and decreasing TN). Amongst the reservoirs with increasing Chl a trends, 68% and 0% have increasing and decreasing POM trends respectively (Table S6). For reservoirs with significant TP trends, less than half have commensurate trends in TN, Chl a and other water quality variables, and notably 9% have contrasting TP and Chl a trends (Table S6). Overall, with the exception of three pairwise combinations (Chl a and POM, TN and POM, PIM and TSS), all other combinations never exceeded 50%. The pairwise combinations with the greatest frequency of contrasting trends were PIM and Chl a (21%) and POM and PIM (20%).

3.4 Co-Variation of Water Color and Water Quality Parameters

All Missouri water quality variables matched in space and time with LimnoSat data are significantly correlated to λ_d (Spearman rank; p < 0.01; Figure S4). Chl a and POM are the least correlated (r = 0.42 and r = 0.42, respectively), and Secchi, TP and PIM are the most correlated (r = -0.67, r = 0.63, and r = 0.63, respectively). To further illustrate these relationships, water quality data were grouped at 10-nm λ_d bins. This analysis yielded statistically significant differences in mean values for all water quality parameters (Kruskal-Wallis; p < 0.05). Subsequent post-hoc pairwise analysis was performed across a spectral range (485-575 nm) that encompassed >98% of data and yields one blue group (485-495 nm) and 8 green groups ending at the green-brown transition (Figure 6). Overall, TP increases with λ_d but there are no statistically significantly differences in the 485-555 nm spectral range; however, waterbodies in the 555-565 nm range have significantly higher TP, that in turn are significantly smaller than TP in waterbodies in the 565-575 nm range (Figure 6A). A similar pattern emerges for TN (Figure 6B) and TSS (Figure 6D), with the exception that

elevated concentrations of both water quality variables in the two green-brown spectral groups (555–575 nm) are not significantly different from each other. Chl a and POM also increase with λ_d , but unlike all other water quality parameters they reach their respective maxima in the 555-565 nm range then decline at longer wavelengths with no statistically significant differences between groups (Figure 6C–E). PIM follows the same relationship to λ_d as TP, whereby the two brownest waterbody groups are significantly different from each other and from the progressively bluer waterbodies (Figure 6F). Secchi depth is the only water quality parameter to form 4 distinct λ_d groups using the conservative post-hoc Bonferroni test (Figure 6G). Similar to TP and PIM, the two brownest spectral end-members constitute two distinct groups, and waterbodies in the 535–555 nm color range are less transparent than bluer (485-535 nm) waterbodies. Finally, DOC has no significant differences across spectral groups but is generally higher in browner, rather than bluer waters (Figure 6H).

To evaluate the correspondence between water color and water quality trends, we calculated alignment scores (Section 2.3 and Table 5) for each reservoir-parameter combination ranging from -1 (consistently opposing trends) to 1 (consistently aligned trends). Across the 22 reservoirs with statistically significant $\Delta \lambda_d$, all listed water quality variables had positive alignment scores (i.e., alignment by variable in Table 5). PIM and Secchi depth had the highest alignment scores (0.59) and 50% of these reservoirs with significant $\Delta \lambda_d$ had statistically significant PIM and Secchi depth trends. POM (0.14) and Chl a (0.07) had the lowest alignment scores. This is broadly consistent with the absence of statistically significant differences across spectral groups, and notable declines in these parameters above 560 nm (Figure 6). Across the 22 reservoirs, 17 had positive alignment scores (i.e., alignment by reservoir in Table 5) such that 77% of reservoirs with significant $\Delta \lambda_d$ showed an aggregated change in water quality variables in a manner consistent with the overall correlations to λ_d . However, 5 of the 22 reservoirs (23%) had negative alignment scores that ran counter to expectations. Notably, all negative alignment scores occurred in browning reservoirs (i.e., positive $\Delta\lambda d$). Amongst these reservoirs, the three with the largest $\Delta\lambda_d$ (Hylak id 1058918, 1057344, 1055671) are all eutrophic systems located in agricultural watersheds, with mean λ_d values > 540 nm (Figures S5–S7). In these reservoirs, Chl a is decreasing, consistent with the observed non-significative decline in this parameter towards the brown end of the spectrum (Figure 6C). The fourth reservoir with a negative alignment score (Hylak id 112285) is also eutrophic and located in an agricultural watershed, though unlike the other reservoirs, PIM shows a modest decline (Figure S8). The fifth reservoir (Hylak id 112606) has the most negative alignment score (-0.86) and is an oligotrophic system located in a forested watershed (Figure S9), where small but significant improvements in water quality contrast with a shift toward browner water color.

4 Discussion

The dominant wavelength (λ_d) can be readily derived from a wide array of Earth-observing satellites, and water color is perhaps the most easily understood indicator of water quality among non-experts. In this study, we combine λ_d from LimnoSat dataset (Topp et al., 2020) with detailed field-based measurements from long-term water quality monitoring programs to investigate changes in both remotely sensed water color and *in situ* measurements of water quality across Missouri reservoirs. The vast majority of reservoirs across the state are currently green, and overall they are closer to the brown rather than blue color threshold. Nonetheless, important spatial patterns are present. Reservoirs in the largely forested Ozark Highlands are bluer than those in agriculturally dominated ecoregions, consistent with the statewide spatial gradients in nutrient enrichment previously described (Jones et al., 2008b). Nearly one-third of the study reservoirs displayed trends in water color, of which approximately 60% shifted toward shorter λ_d (n = 91; bluer), suggesting that recoveries from more turbid and eutrophic conditions are slightly more common than eutrophication across the LimnoSat record analyzed here (1984-2020). This is consistent with a global scale $\Delta\lambda_d$ analysis that showed that majority of

inland waterbodies in temperate and boreal regions are also shifting towards shorter wavelengths (Shen et al., 2025).

402 403

404

405 406

407

408

409

410

411 412

413

414 415

416

417

418

419

420 421

422

423

424

425

426

427

428

429

430

431

432

433 434

435

436 437

438

439

440 441

442

443

444

445

We further identified climatic, landscape, and waterbody morphological factors driving the spatial and temporal patterns observed. Water color trends in Missouri reservoirs were primarily associated with hydroclimate (PDSI), landscape features (elevation and urban land cover) and reservoir morphology (shape). Similar to other parts of the world, reservoirs across the Midwestern USA are experiencing intensifying hydroclimatic extremes as a result of climate change. For example, climate projections indicate an increased likelihood of drought events in this region, both in terms of in frequency and magnitude (Strzepek et al., 2010). Interannual variations in hydrometeorological conditions are significantly correlated with λ_d , such that wet years are associated with higher λ_d values (i.e., browner waters) and drought years are associated with lower λ_d values (i.e., bluer waters). Increased runoff during wet conditions transports greater amounts of terrestrially derived substances – both inorganic (e.g., sediments and nutrients) and organic (e.g., dissolved organic carbon) – into reservoirs that collectively shift λ_d to longer wavelengths (De Wit et al., 2016). The effect of hydrological cycles in controlling nutrients (Jones et al., 2008a) and CDOM (Bhattacharya et al., 2022) has been previously explored in Missouri reservoirs, with wet summers increasing watershed-derived inputs. In Missouri, agricultural watersheds tend to have greater soil organic matter stores than forested watersheds (Jones et al., 2008b) that result in elevated terrestrial CDOM in reservoirs (Bhattacharya et al., 2022), particularly during periods of high precipitation. This is consistent with previous studies showing that Missouri reservoirs in agricultural watersheds are more eutrophic than forested watersheds (Jones et al., 2008b), as well as continentalscale patterns showing a high prevalence of green and brown eutrophic waterbodies in agricultural Midwest regions (Oliver et al., 2017). Incorporating ecoregions into the linear mixed-effect model revealed them as important predictors explaining the covariation between PDSI and λ_d . Notably, the effect of PDSI on reservoir color is dampened in the forested Ozark Highlands relative to agriculturally dominated ecoregions. As demonstrated for nutrient criteria in Missouri reservoirs (Jones et al., 2008a), the absence or presence of water level management across reservoirs is likely an important co-factor modulating the hydrometeorological control on water color.

BRT analysis revealed that reservoir morphology and landscape features collectively explained the spatial variation observed in water color trends. Waterbody elevation consistently ranked as the most important predictor, revealing that reservoirs trending toward bluer wavelengths are generally situated at higher elevations compared to those trending toward greener wavelengths, consistent with regional analysis (Cao et al., 2023), with the noted exception of high alpine environments (Oleksy et al., 2022). Urban land cover ranked as the second most important predictor. Although urbanization can increase chemical and thermal pollution in freshwater ecosystems (Grimm et al., 2008), reservoirs tending toward shorter λ_d occurred in regions where urban cover ranged from 20 to 80%. Similarly, Oleksy et al. (2022) found that reservoirs shifting towards bluer waters were primarily located in areas with a higher percentage of urban land cover. A potential explanation is that local management practices during summer months may alter water color without necessarily improving overall water quality. In Missouri, for example, several reservoirs are managed to optimize recreational fisheries by herbicide (e.g., glyphosate) applications (Jones et al., 2022). Interventions such as applications of nutrientcontaining herbicides can reduce Chl a concentrations by suppressing phytoplankton growth via decreased photosystem II efficiency (Lürling and Roessink, 2006), resulting in short-term shifts toward shorter λ_d . However, over the long-term, these treatments may also increase nutrient availability primarily due to the nitrogen and phosphorus content of these chemicals (Reinl et al., 2022). Reservoir morphology (e.g., waterbody elongation ratio) consistently ranked as the third most important predictor. Reservoirs trending toward shorter λ_d (i.e., bluer waters) are generally smaller and more circular (Figure 5C) and also exhibited greater variability

in the magnitude of water color change. This pattern is consistent with findings that smaller waterbodies are more susceptible to shifts in color (Shen et al., 2025).

Changes in water color broadly align with trends in in situ water quality parameters. Co-located λ_d and water quality parameters were significantly related, and reservoirs with diminishing λ_d , TN, TP, PIM, and increasing water transparency are more common than reservoirs with opposite trends. Yet, despite this general correspondence, Chl a and POM, both proxies for phytoplankton biomass, increased rather than decreased in more reservoirs. This finding stands in contrast to previous studies that show declines in λ_d are often associated with reductions in Chl a concentrations (Lehmann et al., 2018). Earlier Missouri water quality analyses found that particulate inorganic matter (PIM) in reservoirs is typically the dominant fraction of total suspended solids (TSS), particularly in agricultural watersheds due to erosion and runoff (Jones et al., 2008b; Jones and Knowlton, 2005). However, more recent studies have found that particulate organic matter (POM) concentrations now exceed those of PIM in these same systems (Petty et al., 2020). Our results support this shift, and demonstrate that a shift from PIM to POM is the most commonly occurring metric of water quality change. The majority of significant trends (both negative and positive) are confined within the green spectral region closer to the brown rather blue spectral end member, and that in these color regions TP, PIM, and Secchi depth but not Chl a nor POM co-vary with λ_d (Figure 6). Taken together, this demonstrates that diminished λ_d can in fact correspond to elevated phytoplankton biomass, likely through a relaxation of light limitation of phytoplankton communities in eutrophic (i.e., nutrient replete) reservoirs as PIM is much more reflective than POM (Babin et al., 2003). This finding also supports that erosion control resulting from the statewide implementation of best management practices (e.g., shoreline stabilization with rock and water willow; Jones et al., 2022) has resulted in diminished PIM and shifts in water color in many reservoirs.

While significant effort has been undertaken to estimate optically active water quality parameters (e.g., Chl *a*, TSS, CDOM) from space (Cao et al., 2018; Ondrusek et al., 2012; Smith and Bernard, 2020), this study contributes to a small but growing body of research demonstrating strong linkages between remotely sensed color and non-optically active trophic status indicators, particularly TN and TP (Li et al., 2017; Qiao et al., 2021; Windle et al., 2025; Xiong et al., 2019). The retrieval of nutrient concentrations from satellite data is feasible because of their strong correlation with optically active constituents, which respond to nutrient enrichment through increases in phytoplankton biomass and associated suspended matter (Li et al., 2017). TN and TP concentrations are key chemical indicators of biological growth and eutrophication in freshwater systems (Paerl et al., 2015, 2014); therefore, monitoring these nutrients is essential for effective water quality assessment and management. To the date, few studies have attempted to retrieve nutrient concentrations directly from satellite data, limiting our ability to effectively monitor nutrient dynamics at large spatial and temporal scales. Future research should further explore advanced modelling techniques, such as machine learning approaches (Zhu et al., 2024), to improve nutrient retrievals from satellite observations and better detect the complex, non-linear relationships between optical properties and nutrient dynamics.

5 Conclusion

Shifts in water color reflect changes in watershed land use and reservoir management practices mediated through changes in particulate inorganic matter, dissolved organic matter and nutrients. Climate projections indicate increasing frequency and intensity of droughts across the study region (Strzepek et al., 2010). Under such conditions, our findings suggest that reservoirs in the Midwest are likely to shift toward shorter wavelengths (i.e., bluing), potentially altering primary productivity and energy transfer within these man-made systems. The observed reduction in brown color reservoirs suggests improvements in water quality in recent years in historically turbid reservoirs. That said, direct water quality data from several of these reservoirs

reveals opposing trends in particulate inorganic (decreasing) and organic matter (increasing), suggesting that a significant fraction of observed reservoir color changes reflects a reduction in light limitation of the phytoplankton community mediated through diminished suspended mineral particles rather than changes in trophic status. The absence of an overall trend, coupled with contrasting reservoir-level water color trends, underscores that local forces, rather than broad regional drivers, are primarily responsible for the observed changes in water color.

Satellite-derived water color offers a practical tool for assessing how upstream land use and local best management practices (BMPs) affect water quality at the reservoir scale. In a time of reduced federal funding for long-term water quality monitoring programs, our findings underscore the value of satellite-based assessments as a cost-effective and scalable approach to monitor water quality trends over time and space. Many remote-sensing products are now freely available, offering a wide range of spatial (1m – 1 km) and temporal (1 – 15 days) resolutions, and therefore can provide critical information on water quality trends even in regions with limited environmental monitoring (Smits et al., 2025). Moreover, monitoring programs can be strategically redesigned to improve data coverage by selecting key site locations and leveraging remote sensing to interpolate data across time and space (Smits et al., 2025). However, we emphasize the continued importance of field-based observations to ensure accuracy, validate remote sensing products, and maintain the integrity of water quality assessments.

Data Availability Statement

The reservoir metadata (IDs and waterbody names) is provided in the Supplementary Material (Table S7). The *in situ* water quality dataset that support the findings of this study are openly available in the Environmental Data Initiative under the following links: https://doi.org/10.6073/pasta/fb18b84f7e5e9d9f23f224e9e6158572 (1984–2018) and https://doi.org/10.6073/pasta/04c5314549c30b280b8dafb9008f8db4 (2019–2020). The water quality profile data are available at https://github.com/richardson-david/MULimnology_reservoirProfileQAQC.

Funding

- This research was supported by NASA grant 80NSSC22K0771 (Remote Sensing of Water Quality) awarded to
 - R.L.N and G.M.S. The data is based on work supported by the Missouri Department of Natural Resources
 - (MDNR), which funds the Missouri Statewide Lake Assessment Program (SLAP), coordinated by the
 - University of Missouri (MU) Limnology Laboratory. Part of the data was also obtained through the Lakes of
 - Missouri Volunteer Program (LMVP) funded by MDNR, whose contributions are gratefully acknowledged. The
 - graphical abstract was produced as part of work supported by the Prairie Fork Conservation Area (PFCA),
- managed by the Missouri Department of Conservation, under funding awarded to L.P.S., R.L.B., and G.M.S.

Acknowledgments

- The authors are deeply grateful to all students and technicians associated with the MU Limnology Lab over the
- years, whose efforts in collecting, processing, and analyzing the water quality data made this research possible.
- We also thank Dr. Xiaoxu Guo for reviewing the BRT analysis code and offering valuable feedback on our
- 524 approach.

References

525

- Babin, M., Morel, A., Fournier-Sicre, V., Fell, F., Stramski, D., 2003. Light scattering properties of marine
- particles in coastal and open ocean waters as related to the particle mass concentration. Limnol Oceanogr 48,
- 528 843–859.
- Bhattacharya, R., Jones, J.R., Graham, J.L., Obrecht, D. V., Thorpe, A.P., Harlan, J.D., North, R.L., 2022.
- Nonlinear multidecadal trends in organic matter dynamics in Midwest reservoirs are a function of variable
- hydroclimate. Limnol Oceanogr 67, 2531–2546.
- Binding, C.E., Jerome, J.H., Bukata, R.P., Booty, W.G., 2007. Trends in water clarity of the lower Great Lakes
- from remotely sensed aquatic color. J Great Lakes Res 33, 828–841.
- Cao, F., Tzortziou, M., Hu, C., Mannino, A., Fichot, C.G., Del Vecchio, R., Najjar, R.G., Novak, M., 2018.
- Remote sensing retrievals of colored dissolved organic matter and dissolved organic carbon dynamics in North
- American estuaries and their margins. Remote Sens Environ 205, 151–165.
- Cao, Z., Melack, J.M., Liu, M., Kutser, T., Duan, H., Ma, R., 2023a. Shifts, Trends, and Drivers of Lake Color
 - Across China Since the 1980s. Geophys Res Lett 50.
- Cao, Z., Melack, J.M., Liu, M., Kutser, T., Duan, H., Ma, R., 2023b. Shifts, Trends, and Drivers of Lake Color
 - Across China Since the 1980s. Geophys Res Lett 50.
- Castagna, A., Vanhellemont, Q., 2025. A generalized physics-based correction for adjacency effects. Appl Opt
- 542 64, 2719.

538

540

- Charifson, D.M., Huth, P.C., Thompson, J.E., Angyal, R.K., Flaherty, M.J., Richardson, D.C., 2015. History of
- Fish Presence and Absence Following Lake Acidification and Recovery in Lake Minnewaska, Shawangunk
- Ridge, NY. Northeast Nat (Steuben) 22, 762–781.
- De Wit, H.A., Valinia, S., Weyhenmeyer, G.A., Futter, M.N., Kortelainen, P., Austnes, K., Hessen, D.O.,
- Räike, A., Laudon, H., Vuorenmaa, J., 2016. Current Browning of Surface Waters Will Be Further Promoted by
- Wetter Climate. Environ Sci Technol Lett 3, 430–435.
- Dodds, W.K., Bouska, W.W., Eitzmann, J.L., Pilger, T.J., Pitts, K.L., Riley, A.J., Schloesser, J.T., Thornbrugh,
- 550 D.J., 2009. Eutrophication of U. S. freshwaters: Analysis of potential economic damages. Environ Sci Technol
- 551 43, 12–19.
- Elith, J., Leathwick, J.R., Hastie, T., 2008. A working guide to boosted regression trees. Journal of Animal
- Ecology.

- Erlandsson, M., Buffam, I., Fölster, J., Laudon, H., Temnerud, J., Weyhenmeyer, G.A., Bishop, K., 2008.
- Thirty-five years of synchrony in the organic matter concentrations of Swedish rivers explained by variation in
- flow and sulphate. Glob Chang Biol 14, 1191–1198.
- Freeman, C., Evans, C.D., Monteith, D.T., Reynolds, B., Fenner, N., 2001. Export of organic carbon from peat
 - soils. Nature 412, 785–785.

- Gardner, J.R., Yang, X., Topp, S.N., Ross, M.R.V., Altenau, E.H., Pavelsky, T.M., 2021. The Color of Rivers.
- Geophys Res Lett 48.
- Grimm, N.B., Faeth, S.H., Golubiewski, N.E., Redman, C.L., Wu, J., Bai, X., Briggs, J.M., 2008. Global
- Change and the Ecology of Cities. Science (1979) 319, 756–760.
- Hongve, D., Riise, G., Kristiansen, J.F., 2004. Increased colour and organic acid concentrations in Norwegian
- forest lakes and drinking water A result of increased precipitation? Aquat Sci 66, 231–238.
- Jeppesen, E., Søndergaard, M., Jensen, J.P., Havens, K.E., Anneville, O., Carvalho, L., Coveney, M.F., Deneke,
- R., Dokulil, M.T., Foy, B., Gerdeaux, D., Hampton, S.E., Hilt, S., Kangur, K., Köhler, J., Lammens, E.H.H.R.,
- Lauridsen, T.L., Manca, M., Miracle, M.R., Moss, B., Nõges, P., Persson, G., Phillips, G., Portielje, R., Romo,
- 568 S., Schelske, C.L., Straile, D., Tatrai, I., Willén, E., Winder, M., 2005. Lake responses to reduced nutrient
- loading An analysis of contemporary long-term data from 35 case studies. Freshw Biol 50, 1747–1771.
- Jones, J.R., Knowlton, M.F., 2005. Suspended solids in Missouri reservoirs in relation to catchment features and
 - internal processes. Water Res 39, 3629–3635.
- Jones, J.R., Knowlton, M.F., Obrecht, D. V., 2008a. Role of land cover and hydrology in determining nutrients
- 573 in mid-continent reservoirs: Implications for nutrient criteria and management. Lake Reserv Manag 24, 1–9.
- Jones, J.R., Obrecht, D., North, R.L., 2022. Influence of fisheries and shoreline management on limnological
- 575 characteristics of three Missouri reservoirs. Inland Waters 12, 354–367.
- Jones, J.R., Obrecht, D. V., Perkins, B.D., Knowlton, M.F., Thorpe, A.P., Watanabe, S., Bacon, R.R., 2008b.
- Nutrients, seston, and transparency of Missouri reservoirs and oxbow lakes: An analysis of regional limnology.
- 578 Lake Reserv Manag 24, 155–180.
- King, T.V., Meyer, M.F., Hundt, S.A., Ball, G., Hafen, K.C., Avouris, D.M., Ducar, S.D., Wakefield, B.F.,
- Stengel, V.S.,, Vanhellemont, Q., 2024. Sentinel-2 ACOLITE-DSF Aquatic Reflectance for the Conterminous
- United States. U.S. Geological Survey data release.
- Leech, D.M., Pollard, A.I., Labou, S.G., Hampton, S.E., 2018. Fewer blue lakes and more murky lakes across
- the continental U.S.: Implications for planktonic food webs. Limnol Oceanogr 63, 2661–2680.
- Lehmann, M.K., Nguyen, U., Allan, M., van der Woerd, H.J., 2018. Colour classification of 1486 lakes across a
- wide range of optical water types. Remote Sens (Basel) 10.
- Li, Y., Zhang, Yunlin, Shi, K., Zhu, G., Zhou, Y., Zhang, Yibo, Guo, Y., 2017. Monitoring spatiotemporal
 - variations in nutrients in a large drinking water reservoir and their relationships with hydrological and
- meteorological conditions based on Landsat 8 imagery. Science of the Total Environment 599–600, 1705–1717.
- Liu, S., Kim, S., Glamore, W., Tamburic, B., Johnson, F., 2024. Remote sensing of water colour in small
 - southeastern Australian waterbodies. J Environ Manage 352.
- Lürling, M., Roessink, I., 2006. On the way to cyanobacterial blooms: Impact of the herbicide metribuzin on the
- competition between a green alga (Scenedesmus) and a cyanobacterium (Microcystis). Chemosphere 65, 618–
- 593 626.

587

590

- Monteith, D.T., Stoddard, J.L., Evans, C.D., De Wit, H.A., Forsius, M., Høgåsen, T., Wilander, A., Skjelkvåle,
- B.L., Jeffries, D.S., Vuorenmaa, J., Keller, B., Kopécek, J., Vesely, J., 2007. Dissolved organic carbon trends
- resulting from changes in atmospheric deposition chemistry. Nature 450, 537–540.
- Mouw, C.B., Greb, S., Aurin, D., DiGiacomo, P.M., Lee, Z., Twardowski, M., Binding, C., Hu, C., Ma, R.,
- Moore, T., Moses, W., Craig, S.E., 2015. Aquatic color radiometry remote sensing of coastal and inland waters:
 - Challenges and recommendations for future satellite missions. Remote Sens Environ.
- Nakagawa, S., Schielzeth, H., 2013. A general and simple method for obtaining R2 from generalized linear
- mixed-effects models. Methods Ecol Evol 4, 133–142.
- Oleksy, I.A., Collins, S.M., Sillen, S.J., Topp, S.N., Austin, M., Hall, E.K., O'Reilly, C.M., Yang, X., Ross,
 - M.R.V., 2022a. Heterogenous controls on lake color and trends across the high-elevation U.S. Rocky Mountain
- region. Environmental Research Letters 17.
- Oleksy, I.A., Collins, S.M., Sillen, S.J., Topp, S.N., Austin, M., Hall, E.K., O'Reilly, C.M., Yang, X., Ross,
- M.R.V., 2022b. Heterogenous controls on lake color and trends across the high-elevation U.S. Rocky Mountain
 - region. Environmental Research Letters 17.
- Oleksy, I.A., Solomon, C.T., Jones, S.E., Olson, C., Bertolet, B.L., Adrian, R., Bansal, S., Baron, J.S., Brothers,
 - S., Chandra, S., Chou, H.M., Colom-Montero, W., Culpepper, J., de Eyto, E., Farragher, M.J., Hilt, S., Holeck,
 - K.T., Kazanjian, G., Klaus, M., Klug, J., Köhler, J., Laas, A., Lundin, E., Parkes, A.H., Rose, K.C., Rustam,
 - L.G., Rusak, J., Scordo, F., Vanni, M.J., Verburg, P., Weyhenmeyer, G.A., 2024. Controls on Lake Pelagic
- Primary Productivity: Formalizing the Nutrient-Color Paradigm. J Geophys Res Biogeosci 129.
- Oliver, S.K., Collins, S.M., Soranno, P.A., Wagner, T., Stanley, E.H., Jones, J.R., Stow, C.A., Lottig, N.R.,
- 2017. Unexpected stasis in a changing world: Lake nutrient and chlorophyll trends since 1990. Glob Chang Biol
- 615 23, 5455–5467.

599

603

607

609

610

- Ondrusek, M., Stengel, E., Kinkade, C.S., Vogel, R.L., Keegstra, P., Hunter, C., Kim, C., 2012. The
- development of a new optical total suspended matter algorithm for the Chesapeake Bay. Remote Sens Environ
- 618 119, 243–254.
- Paerl, H.W., Xu, H., Hall, N.S., Rossignol, K.L., Joyner, A.R., Zhu, G., Qin, B., 2015. Nutrient limitation
- dynamics examined on a multi-annual scale in Lake Taihu, China: Implications for controlling eutrophication
- and harmful algal blooms. J Freshw Ecol 30, 5–24.
- Paerl, H.W., Xu, H., Hall, N.S., Zhu, G., Qin, B., Wu, Y., Rossignol, K.L., Dong, L., McCarthy, M.J., Joyner,
- A.R., 2014. Controlling cyanobacterial blooms in hypertrophic Lake Taihu, China: Will nitrogen reductions
- cause replacement of non-N2 Fixing by N2 fixing taxa? PLoS One 9.
- Petty, E.L., Obrecht, D. V., North, R.L., 2020. Filling in the Flyover Zone: High Phosphorus in Midwestern
- 626 (USA) Reservoirs Results in High Phytoplankton Biomass but Not High Primary Productivity. Front Environ
- 627 Sci 8.
- Qiao, Z., Sun, S., Jiang, Q., Xiao, L., Wang, Y., Yan, H., 2021. Retrieval of total phosphorus concentration in
- the surface water of Miyun reservoir based on remote sensing data and machine learning algorithms. Remote
- 630 Sens (Basel) 13.

- Reinl, K.L., Harris, T.D., Elfferich, I., Coker, A., Zhan, Q., De Senerpont Domis, L.N., Morales-Williams,
- A.M., Bhattacharya, R., Grossart, H.P., North, R.L., Sweetman, J.N., 2022. The role of organic nutrients in
- structuring freshwater phytoplankton communities in a rapidly changing world. Water Res.
- Roulet, N., Moore, T.R., 2006. Browning the waters. Nature 444.
- Schindler, D.W., Hecky, R.E., McCullough, G.K., 2012. The rapid eutrophication of Lake Winnipeg: Greening
- under global change. J Great Lakes Res 38, 6–13.

638

640

- Shen, X., Ke, C.Q., Duan, Z., Cai, Y., Li, H., Xiao, Y., 2025a. Satellite Observations Reveal Widespread Color
 - Variations in Global Lakes Since the 1980s. Water Resour Res 61.
- 639 Shen, X., Ke, C.Q., Duan, Z., Cai, Y., Li, H., Xiao, Y., 2025b. Satellite Observations Reveal Widespread Color
 - Variations in Global Lakes Since the 1980s. Water Resour Res 61.
- 641 Sillen, S.J., Ross, M.R.V., Collins, S.M., 2024. Long-Term Trends in Productivity Across Intermountain West
- Lakes Provide No Evidence of Widespread Eutrophication. Water Resour Res 60.
- 643 Smith, B., Pahlevan, N., Schalles, J., Ruberg, S., Errera, R., Ma, R., Giardino, C., Bresciani, M., Barbosa, C.,
- Moore, T., Fernandez, V., Alikas, K., Kangro, K., 2020. A Chlorophyll-a Algorithm for Landsat-8 Based on
- Mixture Density Networks. Frontiers in Remote Sensing 1.
- Smith, M.E., Bernard, S., 2020. Satellite Ocean Color Based Harmful Algal Bloom Indicators for Aquaculture
- Decision Support in the Southern Benguela. Front Mar Sci 7.
- Smits, A.P., Hall, E.K., Deemer, B.R., Scordo, F., Barbosa, C.C., Carlson, S.M., Cawley, K., Grossart, H.P.,
- Kelly, P., Mammola, S., Pintar, M.R., Robbins, C.J., Ruhi, A., Saccò, M., 2025. Too much and not enough data:
- Challenges and solutions for generating information in freshwater research and monitoring. Ecosphere 16.
- Strzepek, K., Yohe, G., Neumann, J., Boehlert, B., 2010. Characterizing changes in drought risk for the United
- States from climate change. Environmental Research Letters 5.
- Sukristiyanti, S., Maria, R., Lestiana, H., 2018. Watershed-based Morphometric Analysis: A Review. In: IOP
- 654 Conference Series: Earth and Environmental Science. Institute of Physics Publishing.
- Topp, S., Pavelsky, T., Yang, X., Gardner, J., Rossa, M.R. V, 2020. LimnoSat-US: A Remote Sensing Dataset
- 656 for U.S. Lakes from 1984-2020. Zenodo.
- Topp, S.N., Pavelsky, T.M., Dugan, H.A., Yang, X., Gardner, J., Ross, M.R.V., 2021. Shifting Patterns of
- Summer Lake Color Phenology in Over 26,000 US Lakes. Water Resour Res 57.
- Williamson, C.E., Morris, D.P., Pace, M.L., Olson, O.G., 1999. Dissolved organic carbon and nutrients as
 - regulators of lake ecosystems: Resurrection of a more integrated paradigm. Limnol Oceanogr 44, 795–803.
- Windle, A.E., Malkin, S.Y., Hood, R.R., Silsbe, G.M., 2025. Optical water typing in optically complex waters:
- A case study of Chesapeake Bay. Science of the Total Environment 981.

- Xiong, J., Lin, C., Ma, R., Cao, Z., 2019. Remote sensing estimation of lake total phosphorus concentration
- based on MODIS: A case study of Lake Hongze. Remote Sens (Basel) 11.
- Yang, X., O'Reilly, C.M., Gardner, J.R., Ross, M.R.V., Topp, S.N., Wang, J., Pavelsky, T.M., 2022. The Color
- of Earth's Lakes. Geophys Res Lett 49.
- Zhu, L., Cui, T., Runa, A., Pan, X., Zhao, W., Xiang, J., Cao, M., 2024. Robust remote sensing retrieval of key
- eutrophication indicators in coastal waters based on explainable machine learning. ISPRS Journal of
- Photogrammetry and Remote Sensing 211, 262–280.

671

672

673

		Shorter \(\lambda d \)	Longer \lambda d		
	n	Sen's Slope (nm yr ⁻¹)	n	Sen's Slope (nm yr ⁻¹)	
All reservoirs	91	-0.491±0.284	68	0.378 ± 0.250	
Ecoregion					
Ozark Highlands	28	-0.568 ± 0.329	18	0.501 ± 0.266	
Central Irregular Plains	41	-0.440±0.237	27	0.347 ± 0.211	
Western Corn Belt Plains	7	-0.455±0.312	9	0.367 ± 0.377	
Interior River Valleys and Hills	12	-0.554±0.303	12	0.285 ± 0.146	
Mississippi Alluvial Plain	3	-0.304±0.133	2	0.296 ± 0.204	
Mississippi Valey Loess Plains	0	-	0	-	

Table 2: Linear mixed-effect model describing the relationship between dominant wavelength (λ_d ; response variable), Palmer Drought Severity Index (PDSI), and ecoregions in Missouri. The model includes year as a numeric covariate and reservoir ID as a random term. R^2m and R^2c refer to the marginal (fixed effects only) and conditional (fixed and random effects) coefficients of determination (adjusted R^2), respectively. The intercept corresponds to the reference ecoregion (Central Irregular Plains). Coefficients for other ecoregions and interactions are expressed as differences relative to this reference. Values in bold indicate statistically significant relationships (p-value ≤ 0.05).

Fixed effects	Estimates	SE	95% CI	t-values	<i>p</i> -values	R^2m	R^2c
Intercept	702.94	43.70	617.28 - 788.60	16.09	< 0.001	0.180	0.560
PDSI	1.07	0.09	0.89 - 1.25	11.50	< 0.001		
Year	-0.08	0.02	-0.120.03	-3.49	< 0.001		
Interior River Valleys and Hills	-4.70	3.16	-10.90 - 1.51	-1.48	0.138		
Mississippi Alluvial Plain	6.70	15.93	-24.53 - 37.92	0.42	0.674		
Ozark Highlands	-20.51	2.52	-25.4415.58	-8.15	< 0.001		
Western Corn Belt Plains	-5.12	4.12	-13.21 – 2.96	-1.24	0.214		
PDSI:Interior River Valleys and Hills	-0.40	0.20	-0.800.01	-2.02	0.043		
PDSI:Mississippi Alluvial Plain	4.04	3.11	-10.13 - 2.05	-1.30	0.194		
PDSI:Ozark Highlands	-0.88	0.16	-1.200.56	-5.41	< 0.001		
PDSI:Western Corn Belt Plains	-0.30	0.21	-0.71 - 0.11	-1.44	0.151		
Radom effects							
Reservoir identity	13.03						

Table 3: Slopes of Palmer Drought Severity Index (PDSI) on dominant wavelength (λ_d) for each Missouri ecoregion. Slopes were obtained using *emtrends* from the fitted linear mixed-effect model (LMM). Reported values include the estimates \pm standard error (SE), 95% confidence intervals (CI), Wald z-values, and p-values. Values in bold indicate statistically significant relationships (p-value \leq 0.05).

Ecoregion	Slope	SE	95% CI	z-value	p-value
Central Irregular Plains	1.07	0.09	0.89 - 1.25	11.25	<0.0001
Interior River Valleys and Hills	0.66	0.18	0.32 - 1.01	3.76	0.0002
Mississippi Alluvial Plain	-2.97	3.10	-9.05 - 3.12	-0.96	0.3390
Ozark Highlands	0.19	0.13	-0.07 - 0.45	1.41	0.1585
Western Corn Belt Plains	0.77	0.19	0.40 - 1.14	4.06	< 0.0001

Table 4: Sen's slope estimates (mean \pm SD) for overall trend and for reservoirs exhibiting increasing or decreasing trends in water quality parameters. For the overall trend, n indicates the number of reservoirs with at least 10 consecutive years of data. For increasing and decreasing trends, only reservoirs showing significant trends (p-value ≤ 0.05) are included, and n represents the number of such reservoirs. SD is standard deviation. DOC refers to dissolved organic carbon, POM to particulate organic matter, PIM to particulate inorganic matter, TSS to total suspended solids, DO to dissolved oxygen, and wtemp to water temperature.

			Regional Scale			Reservoir Scale				
		Overall trend			Decr	easing trend	Increasing trend			
		n	Sen's Slope (year ⁻¹)	p-value	n	Sen's Slope (year ⁻¹)	n	Sen's Slope (year ⁻¹)		
Biogeochemical										
Chlorophyll a	μg/L	130	0.286	<0.001	7	-1.37±1.26	36	1.59 ± 1.81		
Secchi depth	m	130	-0.001	0.609	16	-0.05 ± 0.04	18	0.05 ± 0.04		
Total nitrogen (TN)	μmol/L	130	0.108	0.118	19	-0.82 ± 0.54	17	1.21 ± 1.02		
Total phosphorus (TP)	μmol/L	130	0.004	0.258	29	-0.03 ± 0.02	15	0.11 ± 0.16		
TN/TP	-	130	0.195	0.034	11	-1.09±0.76	22	1.33 ± 1.30		
DOC	μmol/L	45	-3.368	0.484	3	-16.4±4.84	2	13.0 ± 4.07		
POM	mg/L	127	0.043	<0.001	7	-0.20±0.29	42	0.16 ± 0.17		
PIM	mg/L	127	-0.054	<0.001	30	-0.14 ± 0.17	13	0.28 ± 0.20		
TSS	mg/L	127	-0.006	0.833	14	-0.27±0.29	20	0.33 ± 0.31		
POM/TSS	-	127	0.006	<0.001	9	-0.02 ± 0.01	56	0.01 ± 0.01		
PIM/TSS	-	127	-0.006	<0.001	56	-0.01±0.01	9	0.02 ± 0.01		
Epilimnion DO	mg/L	70	-0.022	0.208	5	-0.16±0.10	5	0.12 ± 0.08		
Hypolimnion DO	mg/L	70	-0.032	0.001	17	-0.12 ± 0.10	1	0.19 ± 0.00		
Physical										
Surface wtemp	°C	83	0.050	0.010	1	-0.22 ± 0.00	21	0.16 ± 0.12		
Buoyancy frequency	s ⁻²	83	$2x10^{-4}$	<0.001	0	-	39	5x10 ⁻⁴ ±9.3x10 ⁻⁴		
Thermocline depth	m	82	0.019	0.002	7	-0.08 ± 0.06	10	0.10 ± 0.09		
Hypolimnion wtemp	°C	83	-0.044	0.004	14	-0.29±0.37	8	0.27 ± 0.18		
Oxycline depth	m	70	-0.003	0.659	2	-0.10±0.03	2	0.11 ± 0.01		
Hypoxycline depth	m	62	0.004	0.634	11	-0.10 ± 0.07	2	0.13 ± 0.07		

Table 5: Sen's slope estimates for all reservoirs showing significant changes in water color $(\Delta\lambda_d)$ and co-located water quality data. Reservoirs are ordered from decreasing to increasing $\Delta\lambda_d$. Bold values indicate water quality trends (i.e., slopes) in the same direction as $\Delta\lambda_d$ (or the opposite direction for Secchi depth), and * indicates statistically significant trends (*p*-value ≤ 0.05). Alignment scores by reservoir are shown in the rightmost column, and alignment scores by water quality variable are shown in the bottom row. These scores range from 1 (i.e., all significant trends in the same direction as $\Delta\lambda_d$) to -1 (i.e., all significant trends in the opposite direction of $\Delta\lambda_d$).

Reservoir II	D	$\Delta \lambda_{\rm d}$ (nm/yr)	ΔTP (mM/yr)	ΔTN (mM/yr)	ΔSecchi (m/yr))	ΔTSS	ΔChl a (mg/L/yr)	ΔPOM (mg/L/yr)	ΔPIM (mg/L/yr)	Alignment by reservoir
Hylak_id	MU	(11117) 1	(IIIIVII JI)	(IIIIVI J1)	(111 91))	(IIIg/L/y1)	(mg/L/y1)	(IIIg/ E/ J1)	(IIIg/L/J1)	(-1 to 1)
Shorter Ad (i.e	e. Bluer)									
1057422	120	-3.2	-0.05*	-1.49*	0.03*	-0.21*	0.54	0.17	-0.42*	0.57
1057787	10	-2.4	-0.03	-0.96*	0.07	-0.23	-0.06	-0.03	-0.17	0.57
1057880	11	-1.4	-0.03	-2.10*	0.03	-0.17	-0.74	-0.14*	-0.10*	0.71
112563	21	-1.4	-0.02	-0.78*	0.16*	-0.14	-0.25*	-0.04	-0.08	0.71
1058375	110	-1.3	-0.02*	-0.14	0.05*	-0.16*	0.00	-0.01	-0.16*	0.64
1057184	65	-0.9	-0.01	-0.45	0.02	0.04	-0.80	0.11	-0.08	0.21
112432	9	-0.5	-0.05	-0.97*	0.01*	-0.60*	-0.67	-0.01	-0.64*	0.79
1057406	118	-0.5	0.01	-0.28	0.01*	-0.08*	0.73	0.06	-0.19*	0.29
Longer Ad (i.e. B	rowner)									
112285	47	0.2	-0.01*	0.13	-0.00	-0.01	-0.12	0.04	-0.05*	-0.36
112606	39	0.3	-0.00*	-0.20*	0.03*	-0.01*	-0.02	-0.01*	-0.01	-0.86
112223	48	0.6	0.01	0.07	-0.00	-0.02	0.30*	0.04*	-0.04	0.36
1055628	84	0.6	0.06	0.02	-0.03	0.54	0.08	0.05*	0.44	0.57
1055671	180	0.7	-0.02*	-1.17*	-0.01	-0.14*	-1.32*	-0.16*	0.03	-0.57
1055740	137	1.0	0.00	0.63	-0.01	0.44	0.74	0.13	0.26	0.50
1057344	241	1.0	-0.01	-1.17*	-0.03*	0.31	-1.23*	-0.13*	0.38*	-0.14
112102	181	1.2	0.02*	-0.02	-0.03	0.11	0.32	0.00	0.09*	0.50
1058652	186	1.3	0.22*	3.92*	-0.08*	0.82*	5.72*	0.63*	0.15*	1.00
9207	46	1.3	0.06	0.63	-0.04*	0.46*	0.06	0.00	0.50*	0.57
1058918	94	1.3	-0.02	0.52	-0.00	0.04	-0.74*	-0.04	0.06	-0.14
1055538	182	1.5	0.02	0.65*	-0.06*	0.11	0.38	0.10*	0.02	0.71
1055629	185	1.6	0.06*	-0.52	-0.03*	0.44*	-0.80*	-0.06	0.44*	0.29
1055923	50	3.5	0.12*	-0.22	-0.13*	0.54	0.92	0.01	0.59*	0.57
Alignment by varia	able		0.30	0.32	0.59	0.39	0.07	0.14	0.59	

Figure captions

705

708

709 710

713 714

715

716 717

718 719

721

722

723

724

725

726

727

728

729

730

731

734 735

736

739

- Figure 1: Map of (A) Missouri (United States) reservoirs showing available in situ and/or LimnoSat time series 706 707
 - embedded across the state's six Environmental Protection Agency (EPA) ecoregions (Ozark Highlands, Central
 - Irregular Plains, Western Corn Belt Plains, Interior River Valleys and Hills, Mississippi Alluvial Plain, and the
 - Mississippi Valley Loess Plains), and (B) predominant watershed land cover types of the studied reservoirs
 - based on 2021 NLCD data.
- Figure 2: Flowchart illustrating the processing and analysis of climatic (Palmer Drought Severity Index; PDSI), 712
 - remotely-sensed (LimnoSat), in situ water quality (WO), reservoir morphology and watershed land cover data.
 - LMM refers to linear mixed-effect models, BRT refers to boosted regression tree, and n refers to the number of
 - reservoirs included in each dataset or analysis. Water quality parameters include chlorophyll a (chl a), Secchi
 - disk depth (Secchi), total nitrogen (TN), total phosphorus (TP), total nitrogen to total phosphorus ratio (TN/TP),
 - particulate organic matter (POM), particulate inorganic matter (PIM), total suspended solids (TSS), surface
 - water temperature (wtemp), hypolimnion water temperature (hypo wtemp), buoyancy frequency (buoy freq),
 - thermocline depth (thermocline), dissolved oxygen (DO) profile metrics (epilimnion DO, hypolimnion DO,
 - oxycline and hypoxycline), and dissolved organic carbon (DOC).
- 720 **Figure 3:** (A) Distribution of reservoir dominant wavelength (λ_d) across the state's six Environmental
 - Protection Agency (EPA) ecoregions, box and whisker plot of (B) λ_d in recent years (i.e., last year for each
 - reservoir) by ecoregions, (C) dominant wavelength slope (i.e., change; $\Delta \lambda_d$) by ecoregion, (D) λ_d in recent years
 - by watershed land cover types, and (E) $\Delta \lambda_d$ by watershed land cover types. Different letters represent the
 - significant differences (p-values ≤ 0.05) in λ_d and $\Delta\lambda_d$ between ecoregions (B–C) and watershed land cover
 - types (**D**–**E**) based on pairwise Dunn's tests with Bonferroni-adjusted *p*-values.
 - **Figure 4:** (A) Annual mean dominant wavelength (λ_d) for all reservoirs (solid line) and grouped by trend
 - category (increasing and decreasing λ_d ; dashed lines) from 1984 to 2020. Colors correspond to PDSI index:
 - light blue represents moderately wet years (PDSI > 0), dark blue indicates extremely wet years (PDSI $\ge +3$),
 - light brown indicates moderately dry years (PDSI < 0), and dark brown represents extreme drought conditions
 - (PDSI ≤ -3). Graphs (**B**–**D**) represent the number of reservoirs distributed across λ_d (binned in 5 nm intervals) in
 - the first and last years between 1984 and 2020; (**B**) all reservoirs; (**C**) reservoirs trending toward shorter λ_d ; (**D**)
- reservoirs trending toward longer λ_d . Horizontal dashed lines in graphs b-d represent the mean λ_d . 732
- Figure 5: Shapley-based dependence plots for the most important variables selected by the BRT model. Each 733
 - graph shows how the values of a given predictor (x-axis) influence the model's prediction of the dominant
 - wavelength slope ($\Delta \lambda_d$), as represented by the SHAP values (y-axis). Positive SHAP values indicate a
 - contribution to increasing $\Delta \lambda_d$ (brown dots), while negative values indicate a contribution to decreasing $\Delta \lambda_d$
- (green dots) across the study reservoirs. Graphs A-C correspond to different parameters: (A) water body 737
- elevation, (B) urban land cover, and (C) water body elongation ratio. RI refers to average relative importance 738
 - ranked by the selected BRT model. Only significant predictors are shown.
- 740 Figure 6: Box and whisker plot showing the matchups between in situ water quality parameters and dominant
- wavelength (λ_d) values binned in 10 nm intervals. Graphs A–H correspond to different water quality 741
 - parameters: (A) total phosphorus (TP), (B) total nitrogen (TN), (C) chlorophyll a (Chl a), (D) total suspended
 - solids (TSS), (E) particulate organic matter (POM), (F) particulate inorganic matter (PIM), (G) Secchi disk

depth, and (H) dissolved organic carbon (DOC). Different letters within each graph represent significant differences (p-values ≤ 0.05) among λ_d bins based on pairwise Dunn's tests with Bonferroni-adjusted p-values.

744

Figure 1

746

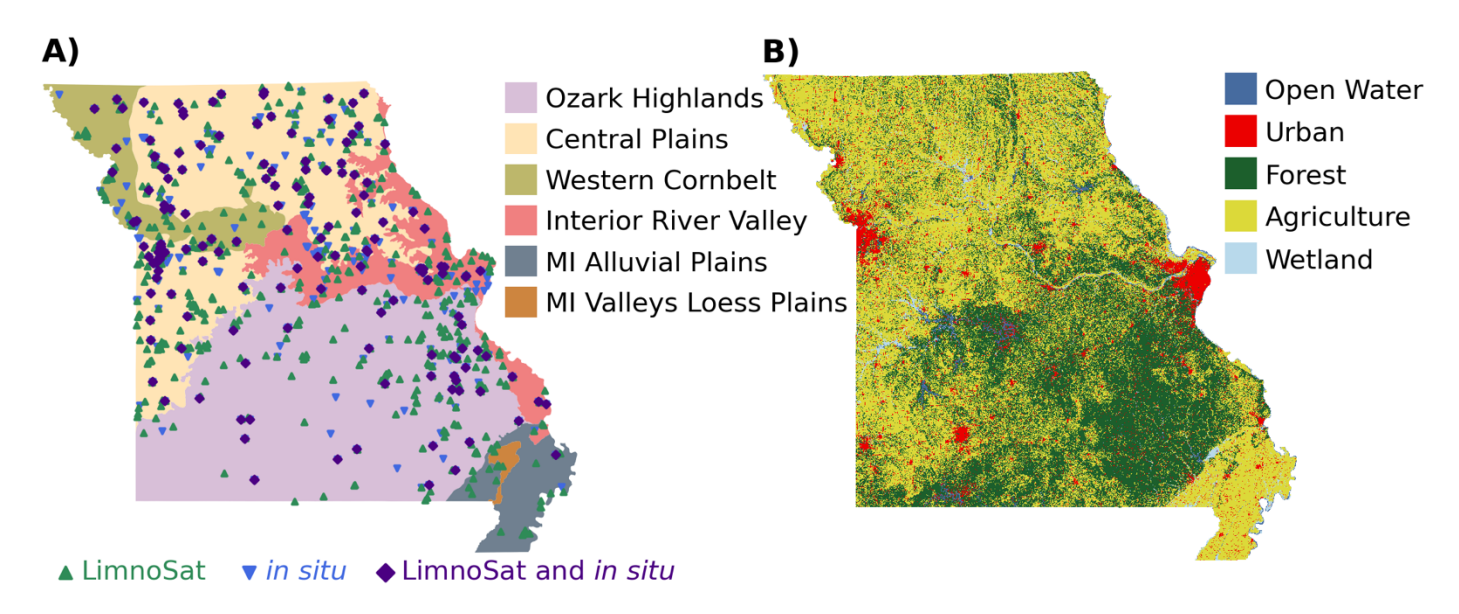


Figure 2

748

749

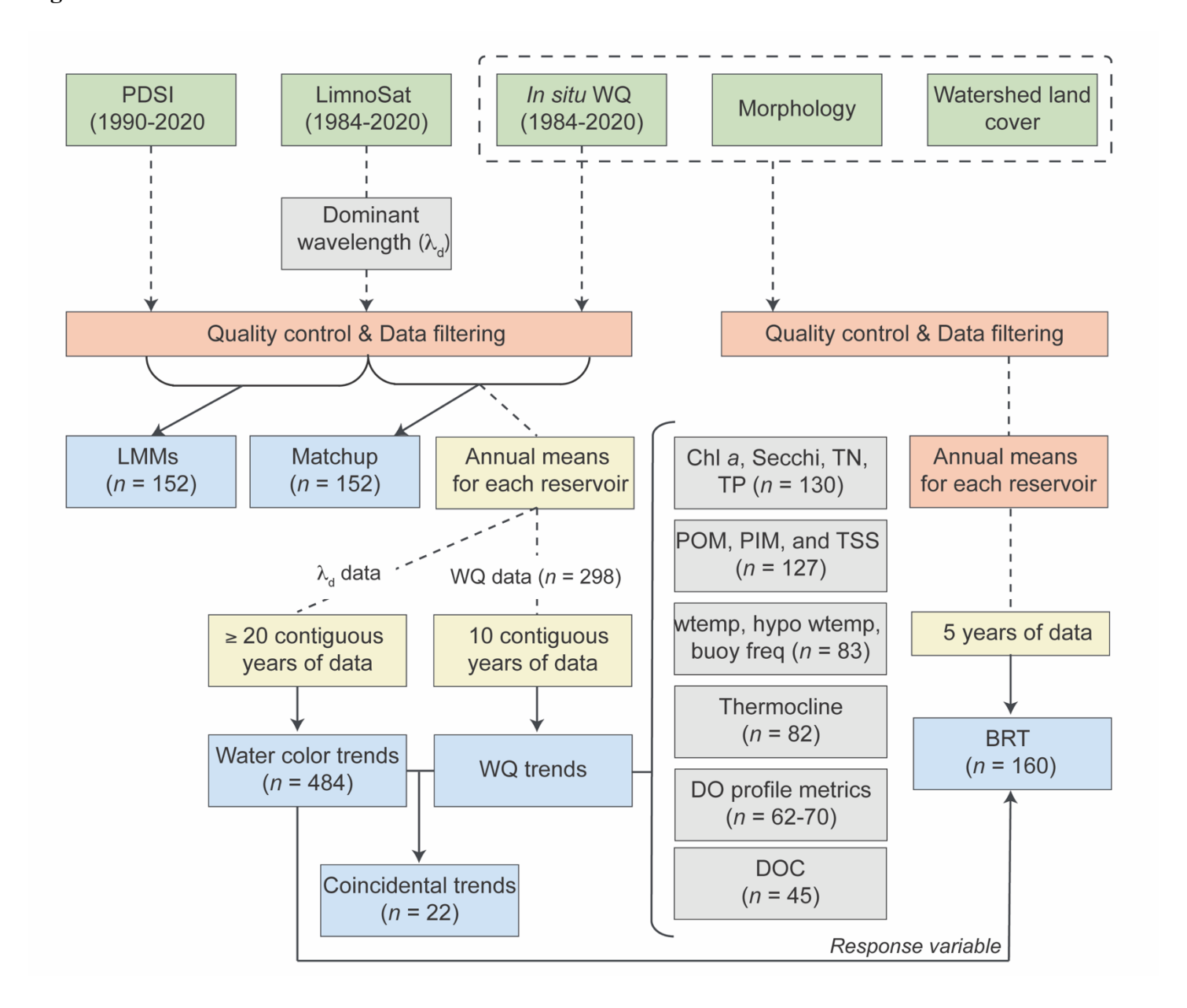


Figure 3

751

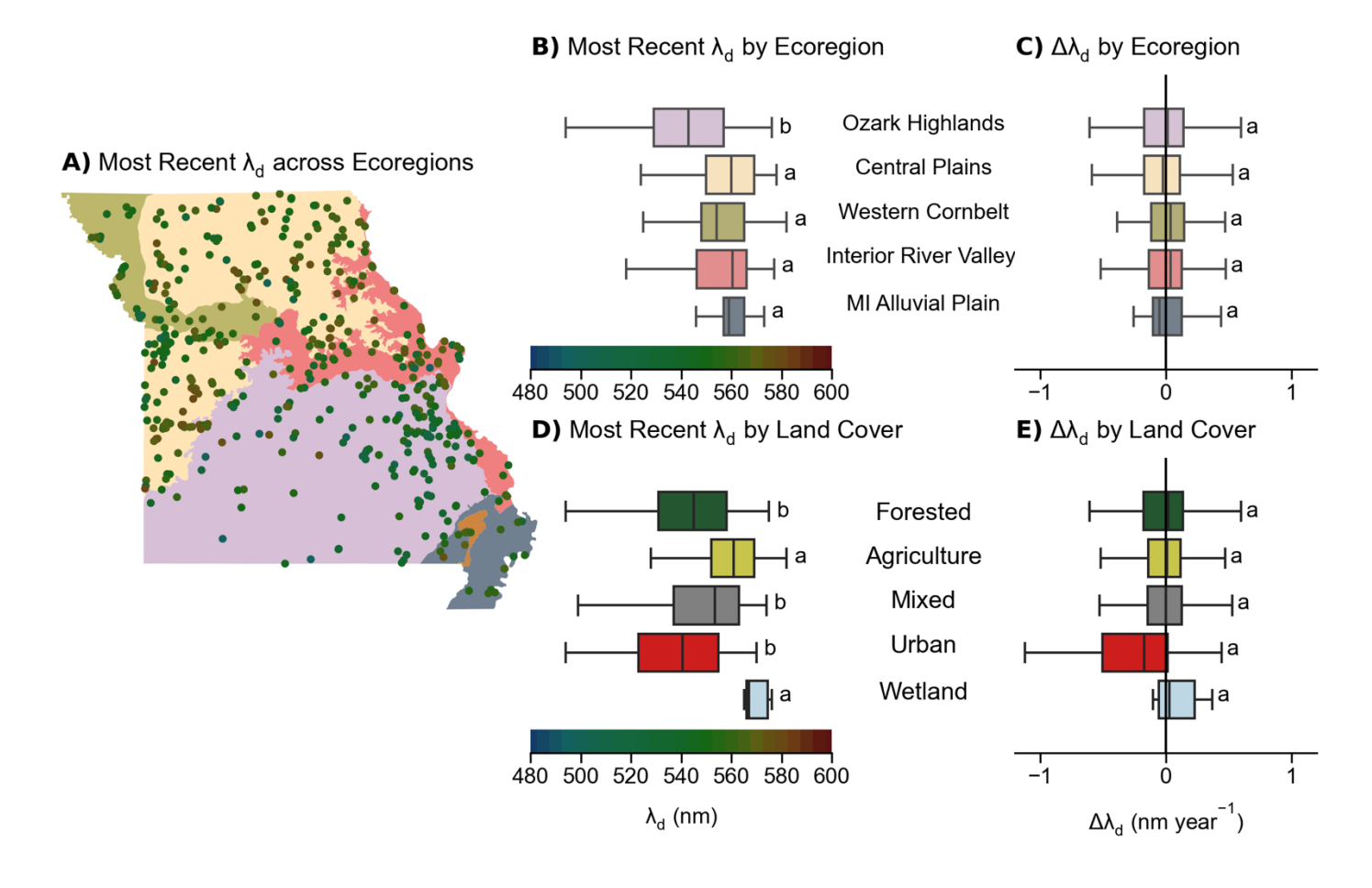


Figure 4

752

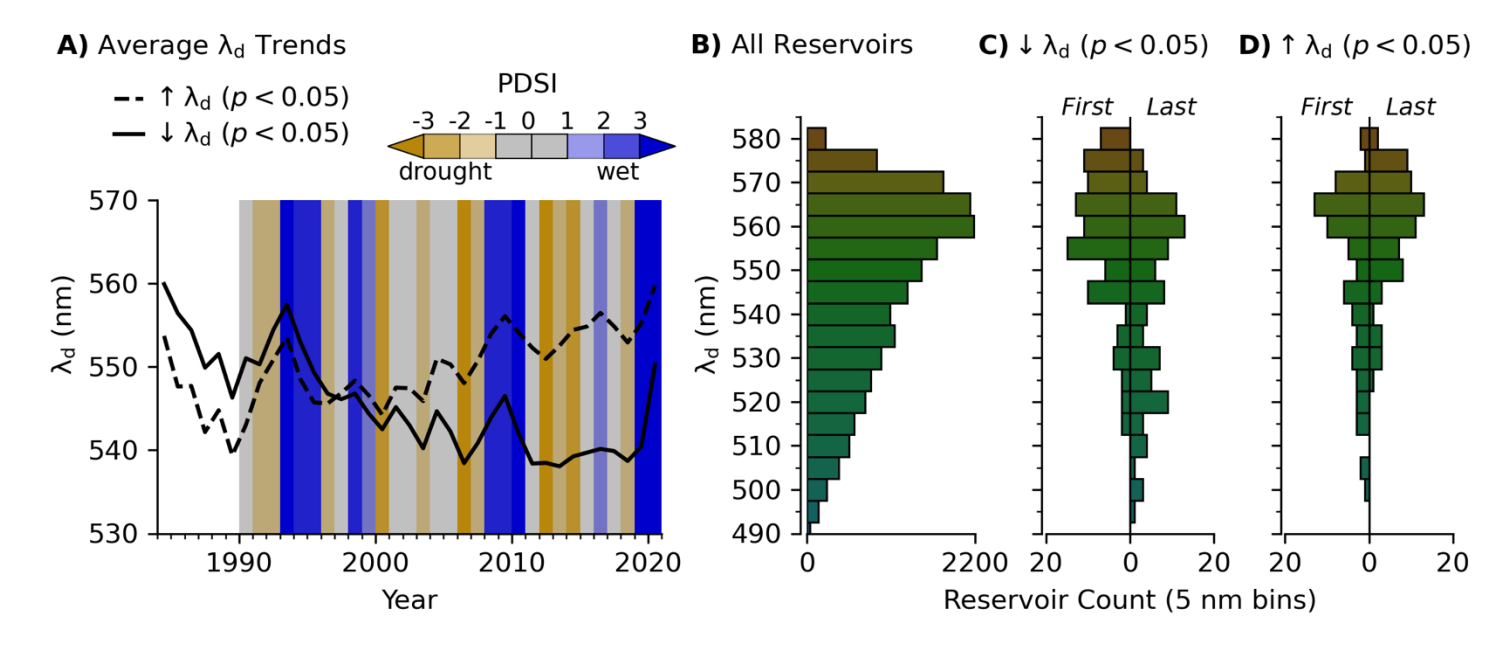


Figure 5

754

755

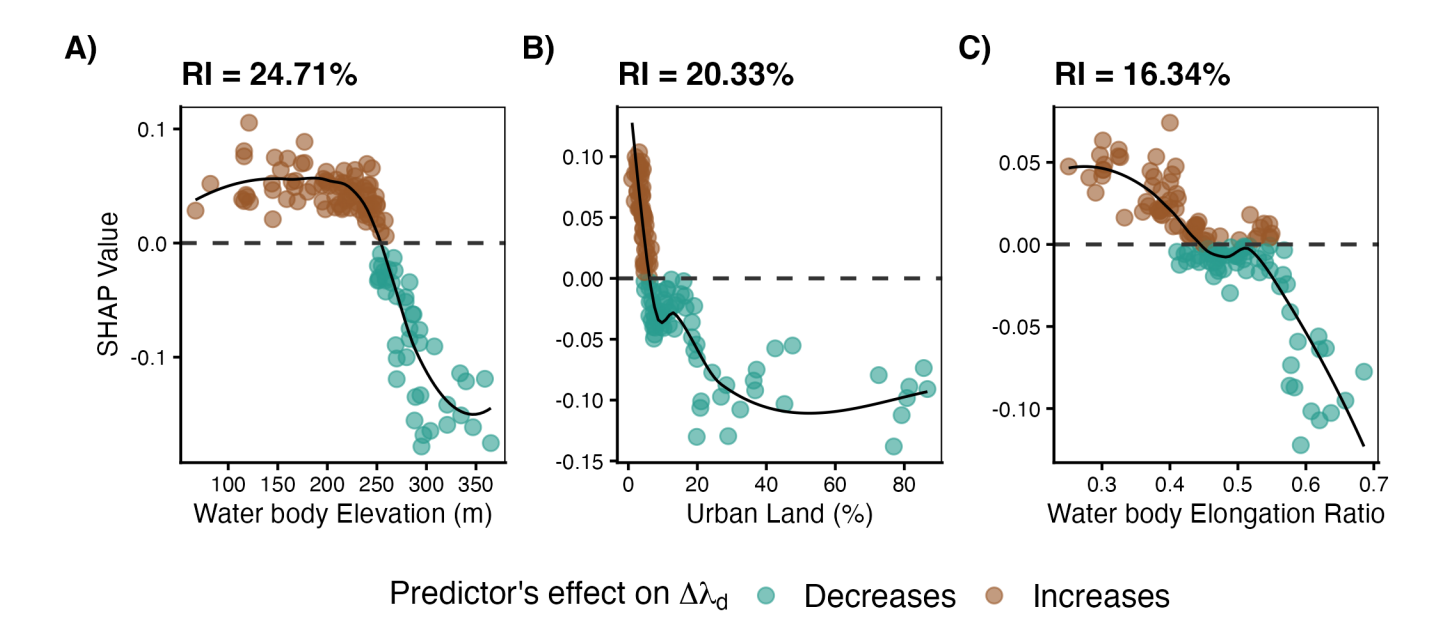
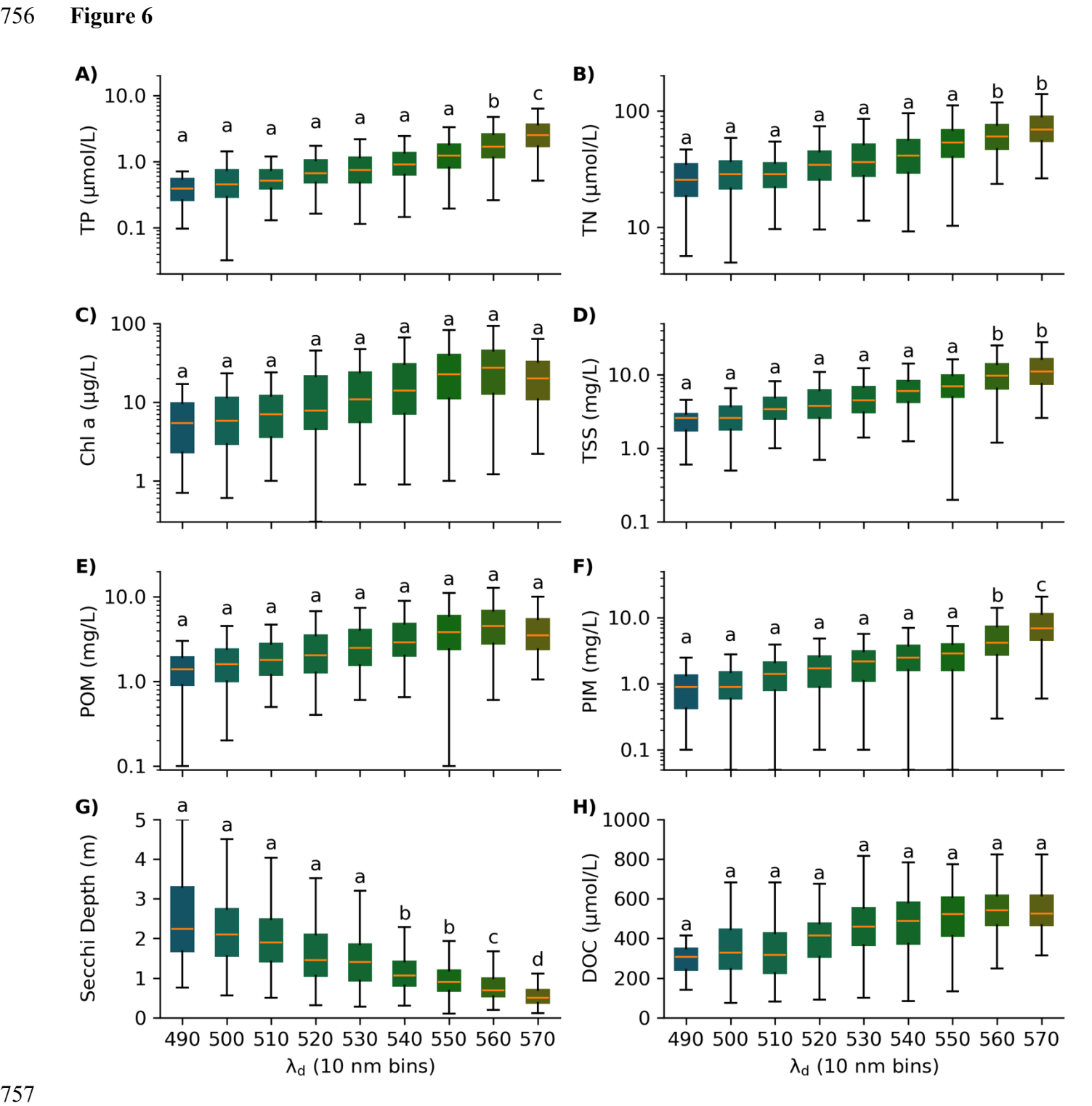


Figure 6



Supplementary Material

Table S1. List of libraries and functions used for the statistical analyses employed in the study.

Analysis	Software	Libraries	Function	Reference
		PySheds		Bartos, 2020
Gaagnatial analysis	Drython	geopandas		Van den Bossche et al., 2024
Geospatial analysis	Python	shapely		Gillies et al., 2022
		numpy		Harris et al., 2020
Brunt-Väisälä buoyancy frequency	R	RLakeAnalyzer		Winslow et al., 2019
		lmerTest		Kuznetsova et al., 2017
Linear mixed-effects	R	parameters		Lüdecke et al., 2020
models	K	lme4	lmer	Bates et al., 2015
		MuMIn	r.squaredGLMM	Bartoń, 2024
Trend analysis	R	trend	sens.slope mk.test	Pohlert, 2020
Boosted Regression	R	dismo	gbm.step	Hijmans et al., 2023
Trees		gbm		Greenwell et al., 2022
Shapley	R	iml		Molnar et al., 2018

Table S2. Instrumentation used for the analysis of water quality parameters in this study (Jones et al., 2024a, 2024b; North et al., 2025).

Parameter	Years	Instrument	Resolution	Accuracy	MDL	Filter Pore Size	Method		
	<2000	YSI 50B	0.1°C	± 0.1°C					
Water Temperature	2000-2006	YSI 85	0.1°C	± 0.1 °C	-	unfiltered	Multiparameter sensor		
Water Temperature	2007-2016	YSI 550A	0.1°C	$\pm~0.2^{\circ}\mathrm{C}$		ummered	with the sensor		
	2017-2020	YSI EXO3	0.001°C	± 0.01°C					
	<2000	YSI 50B		$\pm~0.3~mg/L$					
Dissolved Oxygen	2000-2006	YSI 85	0.01 mg/L	$\pm~0.3~mg/L$		unfiltered	Multiparameter sensor.		
Dissolved Oxygen	2007-2016	YSI 550A	0.01 mg/L	$\pm~0.3~mg/L$	-	ummered	iviumparameter sensor.		
	2017-2020	YSI EXO3		$\pm~0.1~mg/L$					
	< 2018	Turner Designs TD-			0.30 μg/L	1.0 µm, Pall A/E glass fiber filter	Fluorometric analysis following U.S. Environmental Protection Agency method 445.0 (Arar and Collins,		
Total (uncorrected) Chlorophyll	2019-	700 Fluorometer	-	-	0.30 μg/L	0.7 μm GFF	1997), modified using heated ethanol extraction without homogenization (Sartory and Grobbelaar,		
	2020	Cary Eclipse Fluorometer			0.70 μg/L	0.7 μm GFF	1984) and a fluorometer equipped with a flow-through cell (Knowlton, 1984).		
Total Nitrogen	<2020	Genysis 2 Spectrophotometer	1	-	2.500 μmol N/L	unfiltered	Second derivative spectroscopy (Crumpton et al. 1992) following persulfate digestion (APHA, Standard Methods For the Examination of Water and Wastewater (23rd ed). 2017. Method num. 4500-N. C. Nitrogen. DOI: 10.2105/SMWW.2882.086.		
Total Phosphorus	<2020	Genysis 2 Spectrophotometer	-	-	0.032 μmol P/L	unfiltered	Spectrophotometry, persulfate digestion, and ascorbic acid method; APHA, Standard Methods For the Examination of Water and Wastewater (23rd ed). 2017. Method num. 4500-P.B.5.E. Phosphorus. DOI: 10.2105/SMWW.2882.093.		
Total Suspended Solids	<2020	Mettler Toledo model AB54 analytical balance	-	-	0.1 mg/L	1.5 um Whatman glass microfiber	APHA, Standard Methods For the Examination of Water and Wastewater (23rd ed). 2017. Method num. 2540D. Solids. DOI: 10.2105/SMWW.2882.030.		

Particulate Organic Matter						filters, Grade 934- AH	
Particulate Inorganic Matter							
Dissolved Organic Carbon	<2020	Shimadzu TOC- VCPH Analyzer	-	-	0.2 mg/L	1.5 um Whatman glass microfiber filters, Grade 934- AH	High-temperature combustion method; APHA, Standard Methods For the Examination of Water and Wastewater (23rd ed). 2017. Method num. 5310B. Total organic carbon. DOI: 10.2105/SMWW.2882.104
Secchi Depth	<2020	20 cm black/white disk	-	-	0.10 m	unfiltered	-

Table S3. List of references for the statistical analyses employed in the study.

Statistical analysis	Reference				
Linear mixed-effects models	Laird and Ware, 1982				
Sen's slope test	Sen, 1968				
Mann-Kendall trend test	Mann, 1945				
Mann-Kendan trend test	Kendall, 1975				

Table S4. Results of boosted regression trees (BRT), including performance metrics for both training and cross-validated data. Models with missing values are included in the table and reflect cases where convergence was not achieved due to large learning rates or step sizes. Model highlighted in bold is the selected model.

			Trainin	Cross-Validated Data			
Model	Setting	Mean Total Deviance	Mean Residual Deviance	Correlation	R^2	Estimated Deviance	Correlation
Model 1	lr=0.05, tc=1, bg=0.5	-	-	-	-	-	-
Model 2	lr=0.01, tc=1, bg=0.5	0.1	0.07	0.58	28.26	0.09	0.31
Model 3	lr=0.005, tc=1, bg=0.5	0.1	0.07	0.58	28.66	0.09	0.31
Model 4	lr=0.001, tc=1, bg=0.5	0.1	0.07	0.59	30.69	0.1	0.3
Model 5	lr=0.0005, tc=1, bg=0.5	0.1	0.08	0.58	27.26	0.09	0.3
Model 6	lr=0.05, tc=5, bg=0.5	-	-	-	-	-	-
Model 7	lr=0.01, tc=5, bg=0.5	0.1	0.06	0.73	43.77	0.1	0.4
Model 8	lr=0.005, tc=5, bg=0.5	0.1	0.07	0.7	36.64	0.09	0.3
Model 9	lr=0.001, tc=5, bg=0.5	0.1	0.06	0.72	40.66	0.09	0.25
Model 10	lr=0.0005, tc=5, bg=0.5	0.1	0.07	0.7	35.68	0.1	0.28
Model 11	lr=0.05, tc-10, bg=0.5	-	-	-	-	-	-
Model 12	lr=0.01, tc=10, bg=0.5	-	-	-	-	-	-
Model 13	lr=0.005, tc=10, bg=0.5	0.1	0.07	0.7	37.2	0.09	0.42
Model 14	lr=0.001, tc=10, bg=0.5	0.1	0.06	0.72	40.87	0.09	0.33
Model 15	lr=0.0005, tc=10, bg=0.5	0.1	0.07	0.7	34	0.1	0.33
Model 16	lr=0.05, tc=1, bg=0.75	-	-	-	-	-	-
Model 17	lr=0.01, tc=1, bg=0.75	0.1	0.07	0.61	31.08	0.09	0.28
Model 18	lr=0.005, tc=1, bg=0.75	0.1	0.07	0.62	33.92	0.1	0.26
Model 19	lr=0.001, tc=1, bg=0.75	0.1	0.07	0.62	33.44	0.1	0.25
Model 20	lr=0.0005, tc=1, bg=0.75	0.1	0.07	0.61	31.37	0.1	0.32
Model 21	lr=0.05, tc=5, bg=0.75	-	-	-	-	-	-
Model 22	lr=0.01, tc=5, bg=0.75	-	-	-	-	-	-
Model 23	lr=0.001, tc=5, bg=0.75	0.1	0.06	0.76	42.17	0.09	0.32
Model 24	lr=0.001, tc=5, bg=0.75	0.1	0.05	0.79	50.33	0.09	0.31
Model 25	lr=0.0005, tc=5, bg=0.75	0.1	0.06	0.77	43.48	0.09	0.36
Model 26	lr=0.05, tc=10, bg=0.75	-	-	-	-	-	-
Model 27	lr=0.01, tc=10, bg=0.75	-	-	-	-	-	-
Model 28	lr=0.005, tc=10, bg=0.75	0.1	0.06	0.78	44.64	0.1	0.32
Model 29	lr=0.001, tc=10, bg=0.75	0.1	0.05	0.8	50.03	0.09	0.33
Model 30	lr=0.0005, tc=10, bg=0.75	0.1	0.05	0.8	49.86	0.09	0.34

Table S5. Coefficients of determination (R^2) from linear models assessing relationships among coincident water quality trends (i.e. slopes of change), including both significant and non-significant trends. Total phosphorus—TP, total nitrogen—TN, chlorophyll—Chl a, total suspended solids—TSS, particulate organic matter—POM, particulate inorganic matter—PIM, and Secchi depth—Secchi.

	ΔΤΡ	ΔΤΝ	ΔChl a	ΔTSS	ΔΡΙΜ	ΔΡΟΜ	ΔSecchi
ΔТР		0.22	0.12	0.18	0.06	0.17	0.05
ΔΤΝ			0.48	0.39	0.05	0.60	0.09
ΔChl a				0.35	0.09	0.60	0.07
ΔTSS					0.64	0.58	0.23
ΔΡΙΜ						0.08	0.17
ΔΡΟΜ							0.09
ΔSecchi							

Table S6. Percentages of co-occurring water quality trends, expressed as the proportion of total trends observed for each water quality variable. Blue shading indicates co-occurring trends in the same direction (e.g., increasing TP and increasing TN in 31% of reservoirs), whereas red shading indicates contrasting co-occurring trends in opposite directions (e.g., increasing TP and decreasing TN in 3% of reservoirs). Note that Secchi depth follows the opposite interpretation, as increasing trends represent improvements in water transparency.

	ΔТР	ΔTN	ΔChl a	ΔTSS	ΔΡΙΜ	ΔΡΟΜ	ΔSecchi
ΔΤΡ		31	31	38	45	38	2
ΔTN	3		70	36	28	50	8
ΔChl a	9	5		25	9	68	9
ΔTSS	0	5	9		60	48	0
ΔΡΙΜ	4	13	21	4		13	4
ΔΡΟΜ	8	2	0	2	20		6
ΔSecchi	47	29	29	47	47	37	

Table S7. List of reservoirs (*n* = 484) with corresponding identification (Hylak_id and MULakeNumber) and associated ecoregion. NA in MULakeNumber column indicates reservoirs that have Hylak_id and are included in the LimnoSat dataset but are not monitored the water quality programs.

Ecoregion	Hylak_id	MULakeNumber	Hylak_id	MULakeNumber	Hylak_id	MULakeNumber
	9207	46	1056107	NA	1057331	117
	9219	72	1056123	191	1057343	NA
	112053	51	1056147	82	1057344	241
	112111	131	1056153	NA	1057351	166
	112141	133	1056185	NA	1057352	165
	112187	80	1056210	NA	1057369	169
	112214	178	1056231	317	1057396	183
	112223	48	1056241	123	1057406	118
	112254	NA	1056245	81	1057408	NA
	112259	45	1056258	87	1057418	NA
Central Irregular Plains	112285	47	1056261	NA	1057419	NA
Central Irregular Trains	112389	148	1056264	NA	1057422	120
	112394	116	1056285	213	1057442	NA
	112403	67	1056296	211	1057517	NA
	112406	68	1056312	49	1057521	NA
	112425	69	1056317	78	1057539	70
	112429	157	1056341	59	1057575	NA
	112488	90	1056344	139	1057611	62
	112556	NA	1056349	NA	1057641	63
	112557	91	1056359	115	1057662	NA
	1055455	NA	1056376	NA	1057680	266
	1055511	NA	1056378	NA	1057688	NA

1055519	132	1056409	NA	1057700	NA
1055538	182	1056415	88	1057727	NA
1055550	85	1056462	NA	1057743	265
1055553	NA	1056479	NA	1057777	NA
1055589	53	1056505	NA	1057786	NA
1055598	141	1056506	NA	1057808	NA
1055615	NA	1056538	NA	1057812	NA
1055620	NA	1056542	NA	1057819	NA
1055622	NA	1056545	NA	1057854	261
1055628	84	1056563	NA	1057857	NA
1055629	185	1056569	NA	1057870	NA
1055635	NA	1056612	NA	1057914	NA
1055644	NA	1056706	NA	1057928	NA
1055652	NA	1056724	74	1057959	189
1055653	NA	1056766	286	1058026	NA
1055700	NA	1056947	NA	1058110	NA
1055707	83	1056969	NA	1058258	NA
1055719	NA	1056992	NA	1058269	159
1055721	NA	1057006	NA	1058283	NA
1055738	NA	1057019	NA	1058300	NA
1055740	137	1057022	NA	1058322	NA
1055742	NA	1057023	299	1058332	NA
1055761	55	1057087	NA	1058341	NA
1055764	NA	1057090	NA	1058350	NA
1055770	164	1057104	41	1058354	160
1055796	86	1057123	NA	1058361	NA
1055801	56	1057133	NA	1058365	NA

	1055822	57	1057140	NA	1058366	NA
	1055913	NA	1057184	65	1058381	NA
	1055923	50	1057216	NA	1058383	NA
	1055931	NA	1057220	NA	1058393	NA
	1055932	NA	1057230	NA	1058506	NA
	1055940	129	1057242	64	1058512	NA
	1055949	NA	1057248	NA	1058514	NA
	1055955	NA	1057267	NA	1058528	NA
	1055956	NA	1057277	66	1058659	NA
	1055977	NA	1057287	113	1058711	161
	1056004	NA	1057292	NA	1058915	NA
	1056005	222	1057311	NA	1058918	94
	1056008	163	1057315	NA	1058962	NA
	1056011	NA	1057319	NA	1058982	NA
	1056012	130	1057321	NA	1059038	NA
	1056018	114	1057328	NA	1059070	NA
	1056073	NA	1057329	NA		
	9209	145	1057266	NA	1057503	7
	112172	58	1057273	NA	1057513	NA
	112421	6	1057275	NA	1057519	NA
	112432	9	1057330	NA	1057529	403
Interior River Valleys and	112628	NA	1057341	NA	1057545	NA
Hills	1055777	NA	1057342	NA	1057546	442
	1056084	NA	1057347	NA	1057549	NA
	1056088	NA	1057380	NA	1057560	280
	1056274	NA	1057382	NA	1057564	NA
	1056293	NA	1057388	NA	1057567	NA

	T		1			
	1056469	60	1057410	NA	1057577	NA
	1056486	238	1057411	2	1057581	NA
	1056541	NA	1057421	NA	1057619	13
	1056591	NA	1057440	298	1057657	NA
	1056593	NA	1057441	NA	1057671	NA
	1056613	NA	1057444	NA	1057783	NA
	1056684	272	1057455	NA	1058314	NA
	1056777	NA	1057463	293	1058452	NA
	1057007	44	1057467	274	1058544	NA
	1057018	43	1057472	NA	1058660	25
	1057027	NA	1057475	NA	1058926	26
	1057076	NA	1057480	277	1059243	29
	1057126	NA	1057483	NA		
	1057183	5	1057497	NA		
	1059163	NA	1059550	NA	1059719	NA
	1059175	NA	1059599	NA	1059722	NA
	1059438	NA	1059604	NA	1059848	NA
Mississippi Alluvial Plain	1059445	201	1059637	NA	1059854	NA
	1059500	NA	1059652	NA	1059860	NA
	1059519	NA	1059654	NA	1059865	NA
	1059528	NA	1059661	NA	1059870	NA
Mississippi Valley Loess						
Plains	1059530	NA				
	796	89	1058083	NA	1058613	NA
Ozark Highlands	797	149	1058118	NA	1058630	NA
Ozai K Highlanus	804	NA	1058136	NA	1058651	NA
	808	100	1058143	NA	1058652	186

	0269	02	1050172	NIA	1059657	NIA
	9268	92	1058173	NA	1058657	NA
	9273	93	1058196	NA	1058679	NA
	9294	30	1058201	NA	1058685	NA
	9322	101	1058225	NA	1058686	NA
	112542	111	1058228	NA	1058699	NA
	112563	21	1058248	NA	1058707	NA
	112606	39	1058252	NA	1058720	NA
	112627	NA	1058263	NA	1058745	NA
	112679	96	1058264	NA	1058751	NA
	112722	36	1058306	NA	1058752	107
	1057625	184	1058317	NA	1058756	NA
	1057640	12	1058342	NA	1058761	NA
	1057651	306	1058343	NA	1058764	268
	1057666	NA	1058351	NA	1058810	38
	1057702	NA	1058359	NA	1058822	24
	1057703	NA	1058375	110	1058866	NA
	1057711	NA	1058377	NA	1058867	NA
	1057715	NA	1058380	NA	1058895	37
	1057725	420	1058388	NA	1058899	NA
	1057726	NA	1058396	NA	1058943	NA
	1057730	NA	1058418	NA	1058980	146
	1057736	NA	1058419	NA	1059042	NA
	1057750	NA	1058424	22	1059074	NA
	1057756	NA	1058426	40	1059103	95
	1057772	NA	1058436	NA	1059122	28
	1057773	NA	1058440	NA	1059132	NA
	1057774	NA	1058443	NA	1059151	NA

	1057787	10	1058446	23	1059156	NA
	1057809	NA	1058455	NA	1059174	NA
	1057880	11	1058456	267	1059188	NA
	1057889	NA	1058457	NA	1059253	NA
	1057894	NA	1058465	17	1059271	NA
	1057916	NA	1058466	NA	1059301	NA
	1057926	NA	1058478	NA	1059306	NA
	1057931	14	1058489	18	1059311	NA
	1057962	NA	1058490	112	1059328	97
	1057966	NA	1058492	NA	1059392	NA
	1057974	NA	1058493	19	1059402	104
	1057995	NA	1058494	152	1059433	NA
	1058002	NA	1058496	263	1059553	NA
	1058017	NA	1058498	NA	1059554	NA
	1058019	15	1058529	NA	1059628	NA
	1058022	NA	1058534	NA	1059629	NA
	1058023	NA	1058542	NA	1059636	33
	1058044	NA	1058556	271	1059650	NA
	1058064	NA	1058560	NA	1059674	NA
	1058076	310	1058579	NA	1059683	NA
	9219	72	1055930	NA	1056976	NA
	112102	181	1056283	NA	1056984	NA
	112162	NA	1056397	NA	1056988	NA
Western Corn Belt Plains	112163	NA	1056417	NA	1057080	NA
	112221	NA	1056560	NA	1057132	121
	112225	76	1056581	NA	1057151	NA
	112250	NA	1056643	NA	1057168	150

112269	75	1056803	NA	1057178	NA
112284	NA	1056837	NA	1057192	NA
112321	NA	1056843	NA	1057221	162
112362	NA	1056932	155	1057226	NA
1055604	179	1056933	71	1057227	NA
1055671	180	1056943	NA	1057274	NA
1055692	NA	1056965	406		
1055915	NA	1056973	NA		

Table S8. Number of observations (*n*), mean, standard deviation (SD), minimum, and maximum of reservoir catchment characteristics in Missouri.

Ecoregion	Waterbody elevation (m)	Waterbody area (Km²)	Waterbody elongation ratio	Watershed area (Km²)	Watershed elongation ratio	Warea/ Rarea
Ozark Highlands						
n	66	66	66	66	66	66
Mean	232	21.138	0.47	692.73	0.69	136
SD	74	69.395	0.13	1606.03	0.09	417
Minimum	70	0.003	0.16	0.02	0.49	3
Maximum	438	335.495	0.72	7049.67	0.95	3001
Central Irregular Plains						
n	150	150	150	150	150	150
Mean	249	1.076	0.50	27.49	0.68	33
SD	30	2.955	0.10	83.73	0.09	76
Minimum	168	0.004	0.27	0.03	0.35	1
Maximum	318	27.412	0.79	611.22	0.84	883
Western Corn Belt Plains						
n	20	20	20	20	20	20
Mean	262.	3.531	0.47	60.03	0.68	33
SD	35	11.652	0.12	196.10	0.09	41
Minimum	208	0.008	0.23	0.09	0.43	4
Maximum	32	52.598	0.64	887.97	0.81	135
Interior River Valleys and Hills						
n	60	60	60	60	60	60
Mean	187	2.754	0.51	184.06	0.67	110
SD	38	17.715	0.10	1271.22	0.10	524
Minimum	116	0.003	0.29	0.05	0.42	3
Maximum	303	137.612	0.79	9861.20	0.89	4063
Mississippi Alluvial Plain						
n	2	2	2	2	2	2
Mean	80	0.419	0.72	39.51	0.64	64
SD	18	0.302	0.38	54.65	0.18	84
Minimum	67	0.206	0.46	0.87	0.52	4
Maximum	92	0.633	0.99	78.15	0.76	123

Table S9. Number of observations (*n*), mean, standard deviation (SD), minimum, and maximum of biochemical parameters in Missouri reservoirs.

Ecoregion	Chla- <i>a</i> (µg/L)	Secchi depth (m)	TN (µmol N/L)	TP (μmol P/L)	TN/TP (in log)	DOC (µmol/L)	POM (mg/L)	PIM (mg/L)	TSS (mg/L)	POM/TSS	PIM/TSS	Epilimnion DO (mg/L)	Hypolimnion DO (mg/L)
	(F8 2)		(1,1,2)	(1,11,1,1)	(111 10 g)	(10000000000000000000000000000000000000	(((111.8/2)				
Ozark Highlands													
n	66	66	66	66	66	55	64	65	64	64	64	57	57
Mean	9.79	1.76	37.352	0.918	3.858	363.3	2.1	3.0	5.0	0.5	0.5	7.90	2.49
SD	16.87	0.91	23.344	0.967	0.513	134.3	2.3	4.5	5.5	0.2	0.2	1.62	2.66
Minimum	1.00	0.45	7.138	0.204	2.690	83.9	0.3	0.2	0.8	0.1	0.1	3.03	0.00
Maximum	121.50	4.17	112.063	6.135	5.102	707.7	15.6	26.6	30.7	0.9	0.9	12.20	8.97
Central Irregular Plains													
n	150	150	150	150	150	121	150	150	150	150	150	126	126
Mean	24.03	0.98	69.150	2.248	3.584	542.8	4.6	9.6	14.1	0.5	0.5	7.83	1.44
SD	29.05	0.71	42.815	2.178	0.527	106.6	4.1	18.2	21.2	0.2	0.2	2.07	2.12
Minimum	0.60	0.10	28.551	0.226	2.256	278.9	0.6	0.1	1.6	0.1	0.0	3.40	0.00
Maximum	237.70	4.50	299.072	18.986	5.024	899.3	23.5	119.7	138.5	1.0	0.9	15.70	10.30
Western Corn Belt Plains													
n	20	20	20	20	20	13	20	20	20	20	20	14	14
Mean	47.48	1.33	82.138	2.782	3.669	477.5	8.7	9.7	18.4	0.5	0.5	8.73	0.57
SD	80.38	0.94	85.724	4.723	0.559	107.1	16.3	23.2	37.6	0.2	0.2	3.15	0.81
Minimum	2.00	0.10	18.558	0.226	2.759	352.0	1.3	0.9	2.8	0.1	0.2	4.83	0.00
Maximum	323.20	3.60	361.884	20.407	4.964	742.3	61.4	107.0	168.4	0.8	0.9	14.70	3.00
Interior River Valleys and Hills													
n	60	59	60	60	60	28	60	60	60	60	60	32	32
Mean	21.18	1.32	56.379	1.837	3.734	512.7	4.2	7.4	11.6	0.5	0.5	7.37	1.52
SD	33.91	1.07	31.883	2.060	0.665	143.4	4.7	20.5	24.1	0.2	0.2	2.74	2.22
Minimum	0.70	0.10	17.131	0.242	2.186	291.4	0.2	0.1	0.7	0.2	0.0	3.71	0.00
Maximum	168.40	6.76	201.285	10.655	5.015	918.7	26.7	151.2	177.9	1.0	0.0	16.30	9.00
IVIAXIIIIUIII	100.40	0.70	201.203	10.033	5.015	710./	20.7	131.4	1//.9	1.0	0.9	10.30	2.00

<i>Aississippi</i>	Alluvial	Plain
--------------------	----------	-------

n	2	2	2	2	2	0	2	2	2	2	2	1	1
Mean	125.10	0.52	81.370	3.826	3.237	-	11.7	3.3	15.0	0.8	0.2	10.80	4.50
SD	173.52	0.33	82.773	4.407	0.330	-	14.8	4.3	19.2	0.1	0.1	-	-
Minimum	2.40	0.28	22.841	0.710	3.003	-	1.2	0.2	1.4	0.8	0.1	10.80	4.50
Maximum	247.80	0.75	139.900	6.942	3.471	-	22.2	6.3	28.5	0.9	0.2	10.80	4.50

Table S10. Number of reservoirs (*n*), mean, standard deviation (SD), minimum, and maximum of physical parameters in Missouri reservoirs.

Ecoregion	Surface wtemp (°C)	Buoyancy frequency (s ⁻²)	Thermocline depth (m)	Hypolimnion wtemp (°C)	Oxycline (m)	Hypoxycline (m)
Ozark Highlands						
n	58	58	58	58	58	54
Mean	24.1	0.013	3.6	14.3	3.1	5.6
SD	3.3	0.018	1.6	5.5	2.2	2.8
Minimum	16.8	0.002	0.3	7.9	0.1	2.0
Maximum	35.0	0.126	7.5	31.5	9.5	12.0
Central Irregular Plains						
n	126	126	126	126	126	126
Mean	25.1	0.010	2.9	16.8	2.0	3.7
SD	4.4	0.007	1.4	4.5	1.2	1.4
Minimum	15.4	0.000	0.1	7.1	0.1	0.5
Maximum	33.4	0.044	6.5	31.8	7.5	8.0
Western Corn Belt Plains						
n	15	15	14	14	15	14
Mean	25.2	0.008	3.9	15.7	2.3	4.5
SD	2.6	0.004	2.2	3.7	1.0	1.6
Minimum	21.8	0.001	0.8	8.0	0.8	2.0
Maximum	30.9	0.016	8.5	23.1	4.5	8.0
Interior River Valleys and Hills						
n	32	32	32	32	32	32
Mean	23.1	0.013	3.1	13.4	2.8	4.1
SD	4.1	0.019	1.2	5.2	1.7	1.6
Minimum	17.0	0.000	0.1	6.3	0.5	1.5
Maximum	29.4	0.111	5.5	24.2	8.3	9.5
Mississippi Alluvial Plain						
n	1	1	1	1	1	0
Mean	25.8	0.005	0.8	24.4	0.8	-
SD	-	-	-	-	-	-
Minimum	25.8	0.005	0.8	24.4	0.8	-
Maximum	25.8	0.005	0.8	24.4	0.8	_

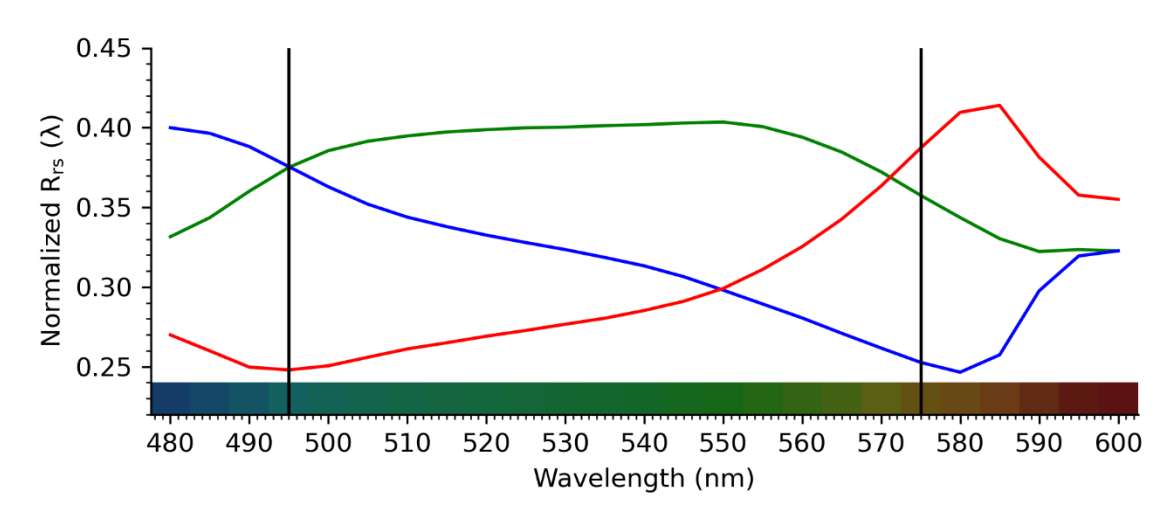


Figure S1: Normalized remote sensing reflectance spectra (R_{rs}) from 480 to 600 nm for three representative color types: blue (blue line), green (green line), and red/brown (red line) reservoirs. The reflectance was normalized to the total area under the curve. Vertical black lines indicate threshold wavelengths at 495 nm and 575 nm, used to delineate broad water color groups defined as blue ($\lambda_d \le 495$ nm), green (495 nm < $\lambda_d < 575$ nm), and brown ($\lambda_d \ge 575$ nm). The color gradient bar represents the perceived color based on the Forel-Ule Index (FUI) color scale, illustrating the hue associated with each wavelength.

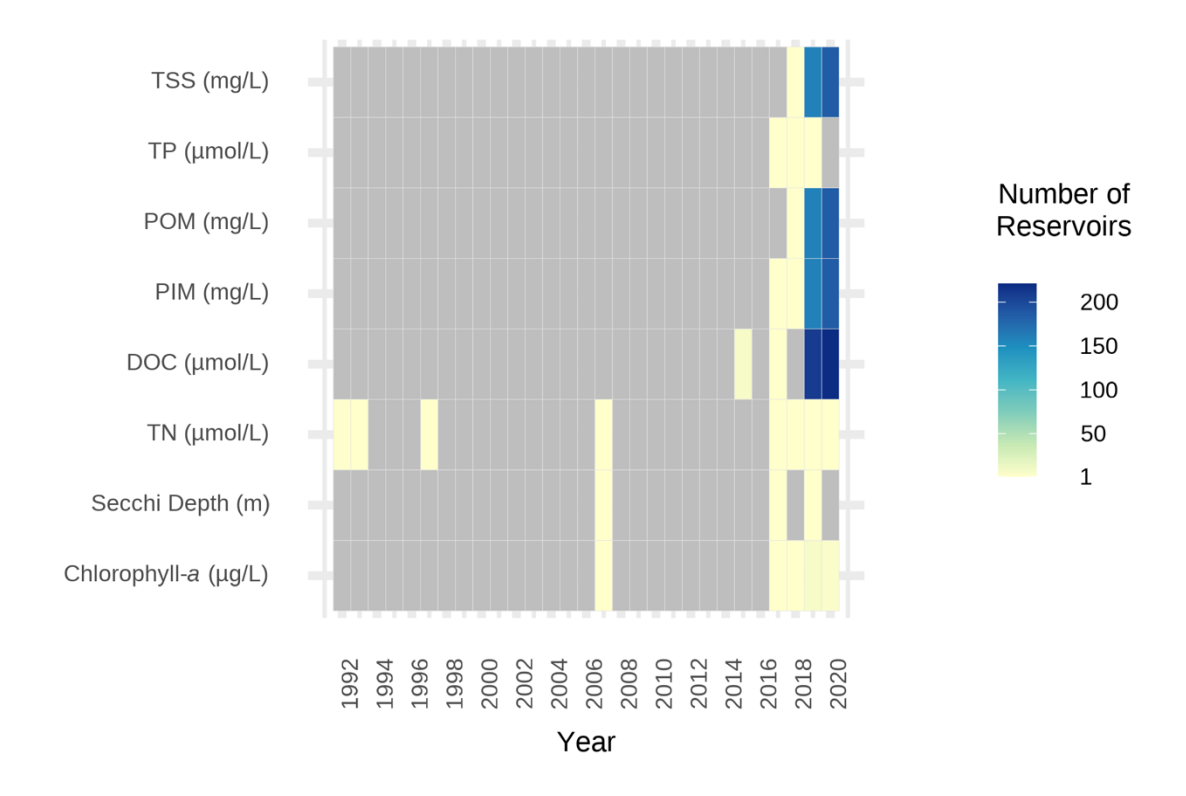


Figure S2: Number of epilimnetic samples used per variable and year when surface samples were not available.

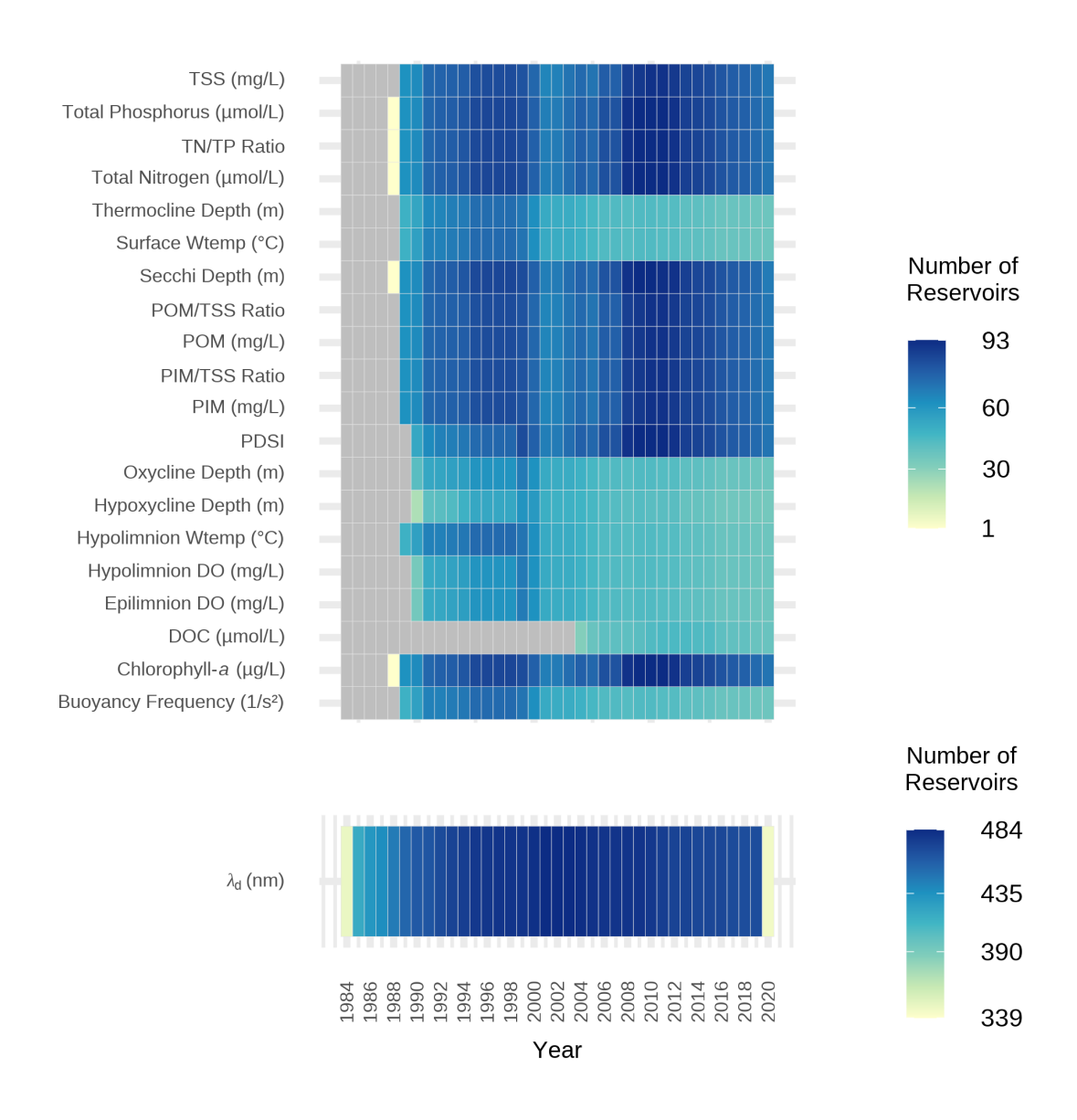


Figure S3: Number of reservoirs per variable and year included in the trend analysis. For dominant wavelength (λ_d) , only reservoirs with a minimum of 20 consecutive years of data between 1984 and 2020 were included. For physical and chemical parameters, the analysis was limited to reservoirs with at least 10 consecutive years within the same period. Gray cells represent missing data.

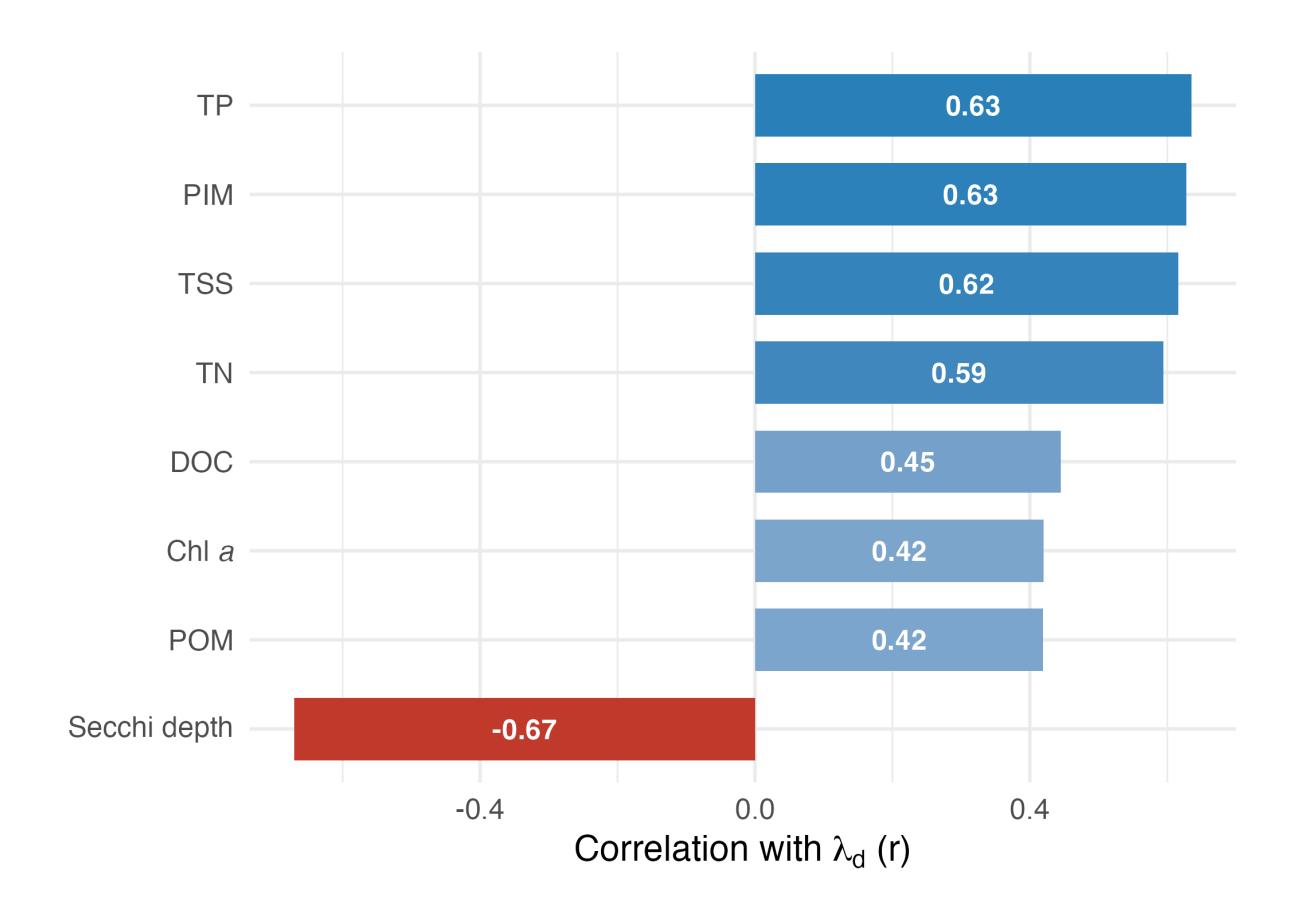


Figure S4: Spearman pairwise correlation between dominant wavelength (λ_d) and the following water quality parameters: total phosphorus (TP), particulate inorganic matter (PIM), total suspended solids (TSS), total nitrogen (TN), dissolved organic carbon (DOC), chlorophyll a (Chla a), particulate organic matter (POM), and Secchi depth.

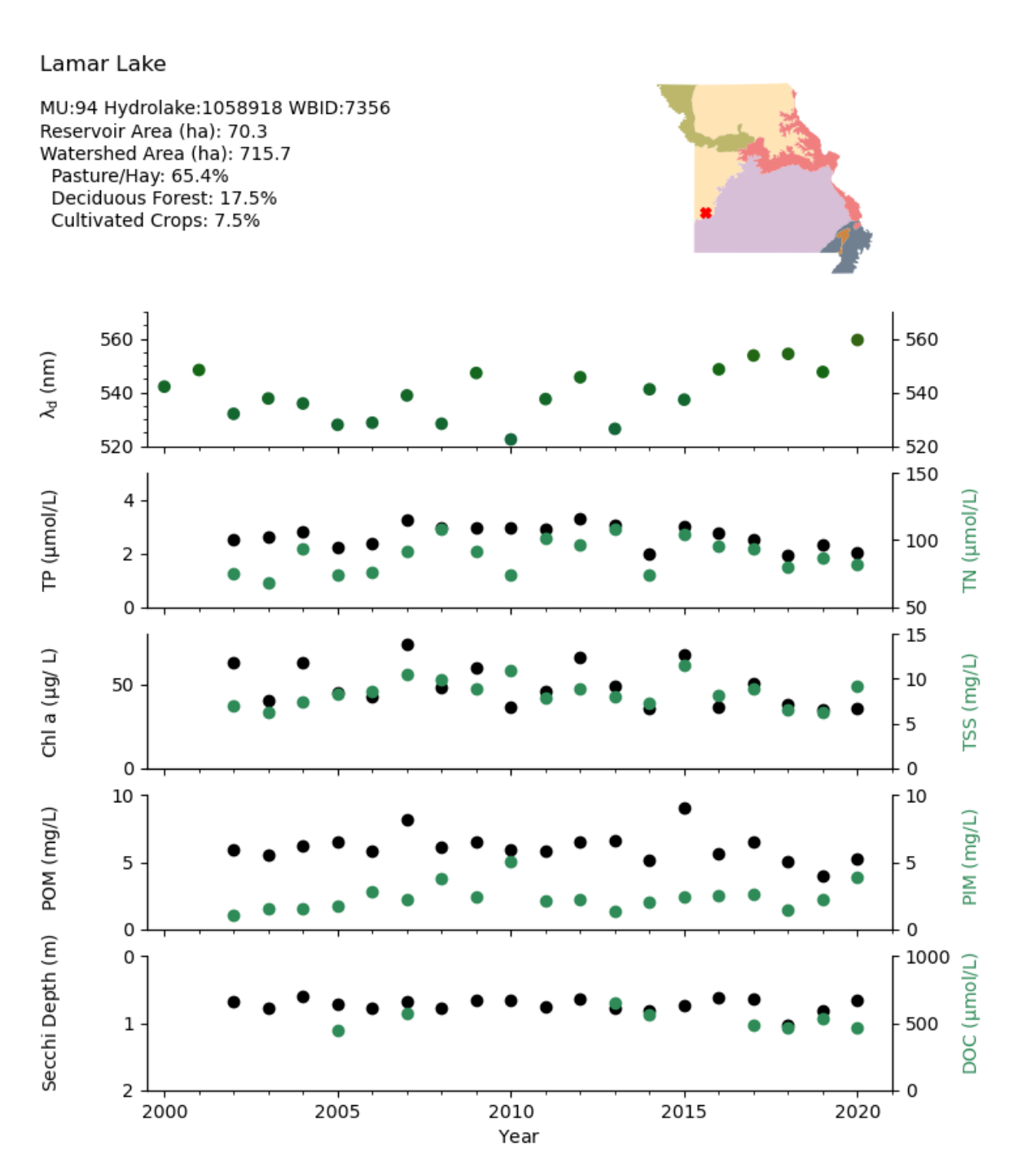


Figure S5: Water color (dominant wavelength; λ_d) and water quality (total phosphorus–TP, total nitrogen–TN, chlorophyll–Chl a, total suspended solids–TSS, particulate organic matter–POM, particulate inorganic matter–PIM, Secchi depth, and dissolved organic carbon–DOC) changes in Lamar Lake (Hylak_id 1058918). Black and green points refer to left and right axes respectively. Chl *a* is significantly decreasing; λ_d is significantly increasing.

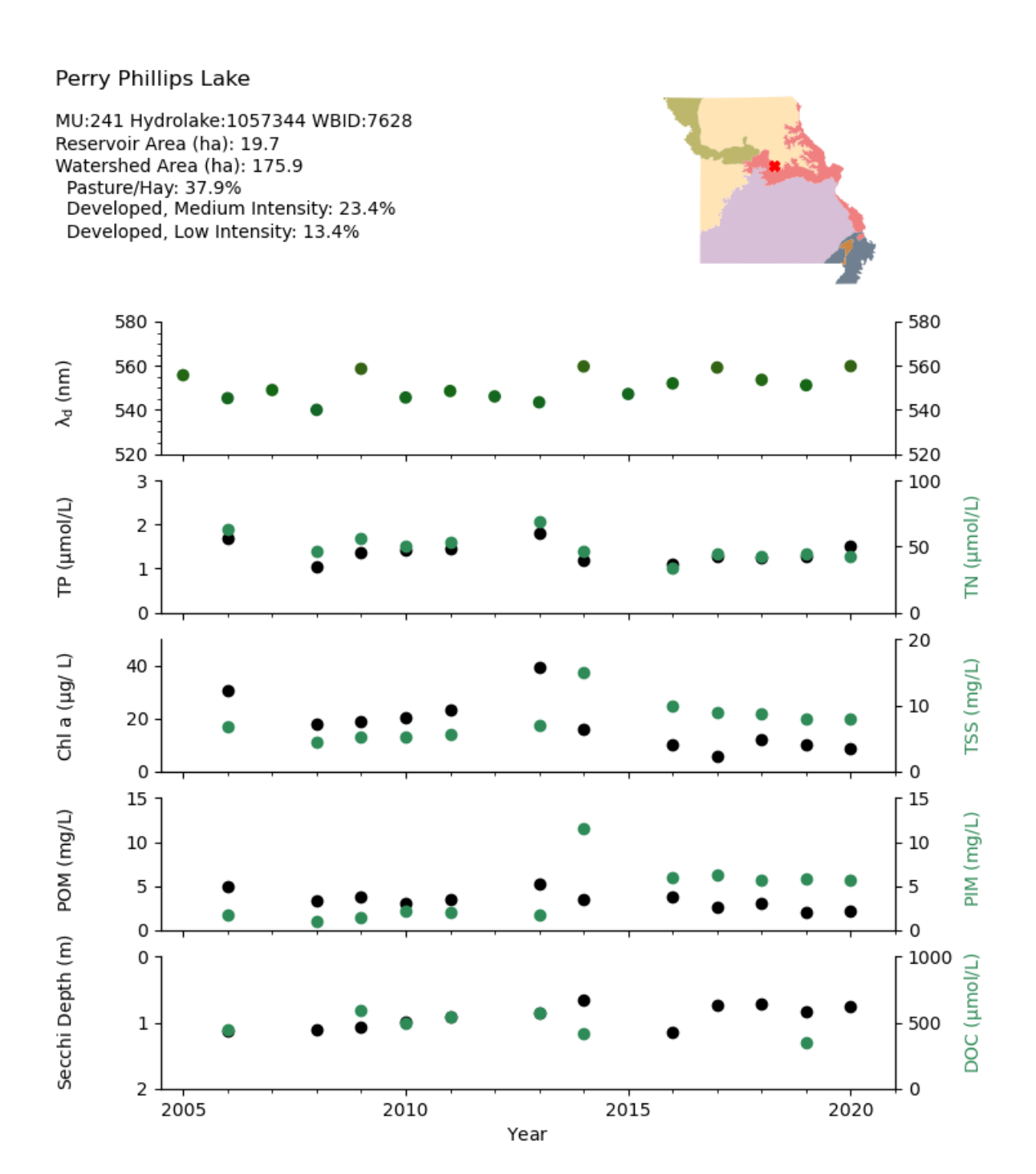


Figure S6. Water color (dominant wavelength; λ_d) and water quality (total phosphorus–TP, total nitrogen–TN, chlorophyll–Chl a, total suspended solids–TSS, particulate organic matter–POM, particulate inorganic matter–PIM, Secchi depth, and dissolved organic carbon–DOC) changes in Perry Phillips Lake (Hylak_id 1057344). Black and green points refer to left and right axes respectively. TN, Secchi, Chl *a*, and POM are significantly decreasing; λ_d and PIM are significantly increasing.

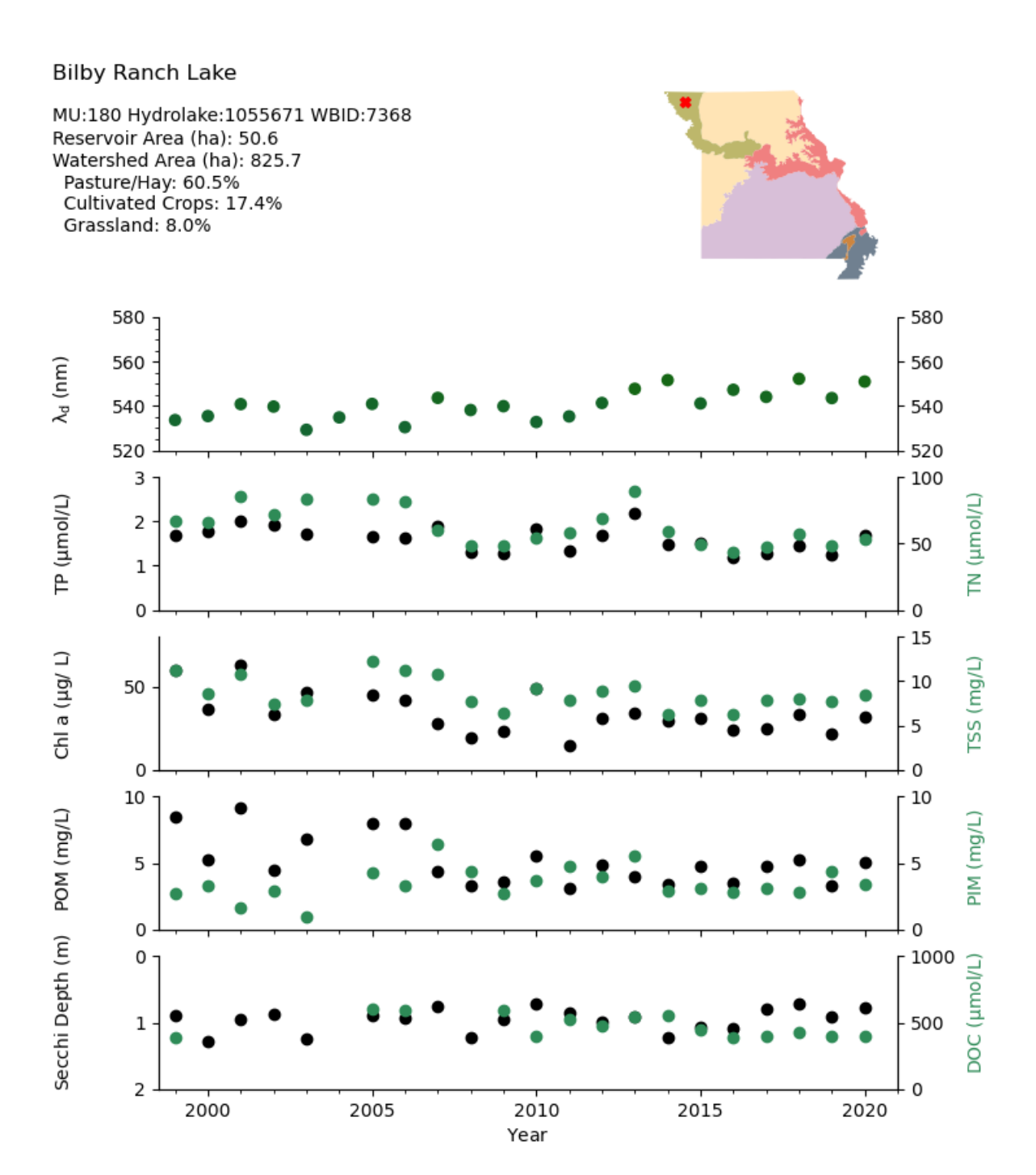


Figure S7. Water color (dominant wavelength; λ_d) and water quality (total phosphorus–TP, total nitrogen–TN, chlorophyll–Chl a, total suspended solids–TSS, particulate organic matter–POM, particulate inorganic matter–PIM, Secchi depth, and dissolved organic carbon–DOC) changes in Billy Ranch Lake (Hylak_id 1055671). Black and green points refer to left and right axes respectively. TP, TN, TSS, Chl *a* and POM are significantly decreasing; λ_d is significantly increasing.

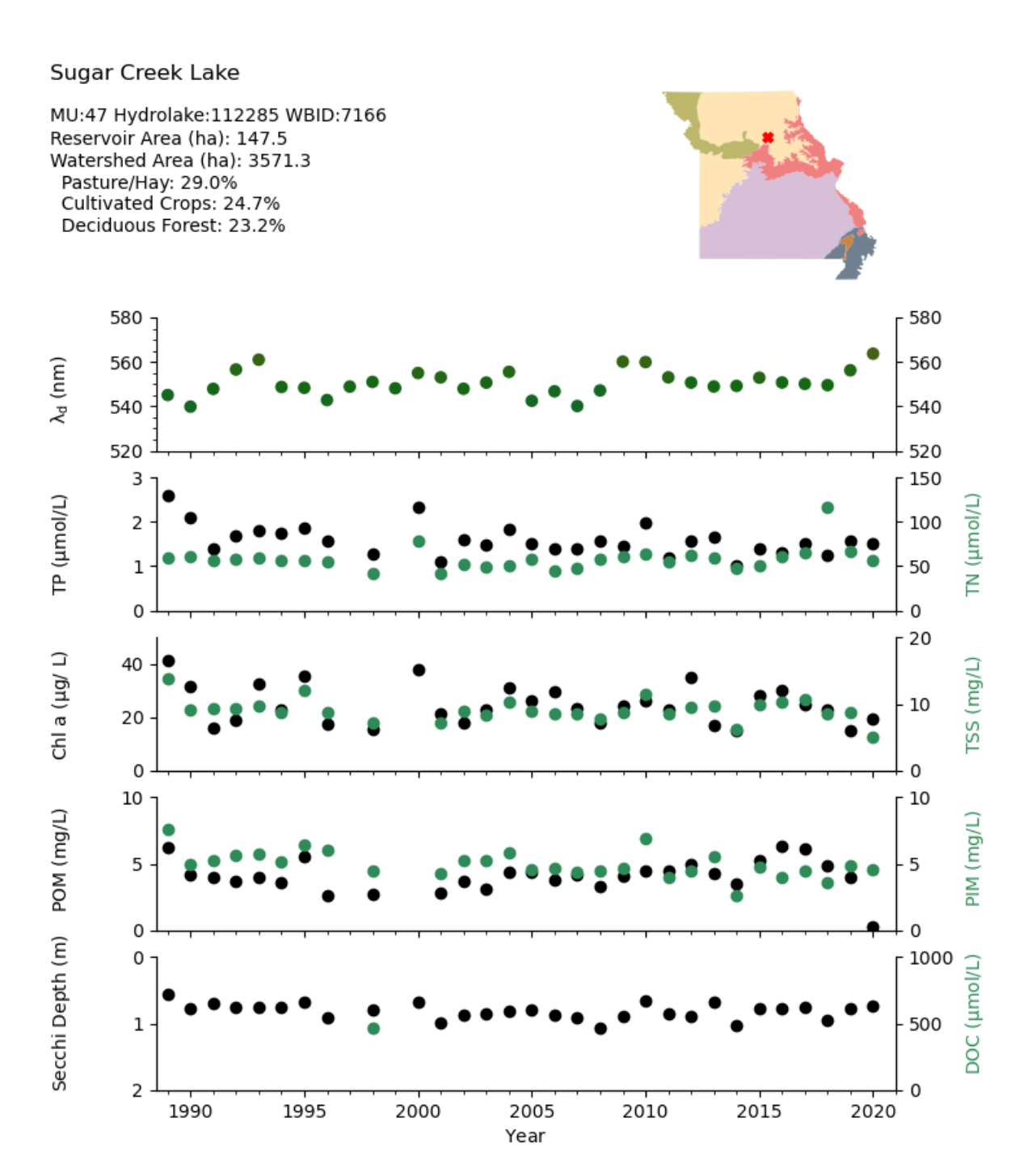


Figure S8. Water color (dominant wavelength; λ_d) and water quality (total phosphorus–TP, total nitrogen–TN, chlorophyll–Chl a, total suspended solids–TSS, particulate organic matter–POM, particulate inorganic matter–PIM, Secchi depth, and dissolved organic carbon–DOC) changes in Sugar Creek Lake (Hylak_id 112285). Black and green points refer to left and right axes respectively. TP and PIM are significantly decreasing; λ_d is significantly increasing.

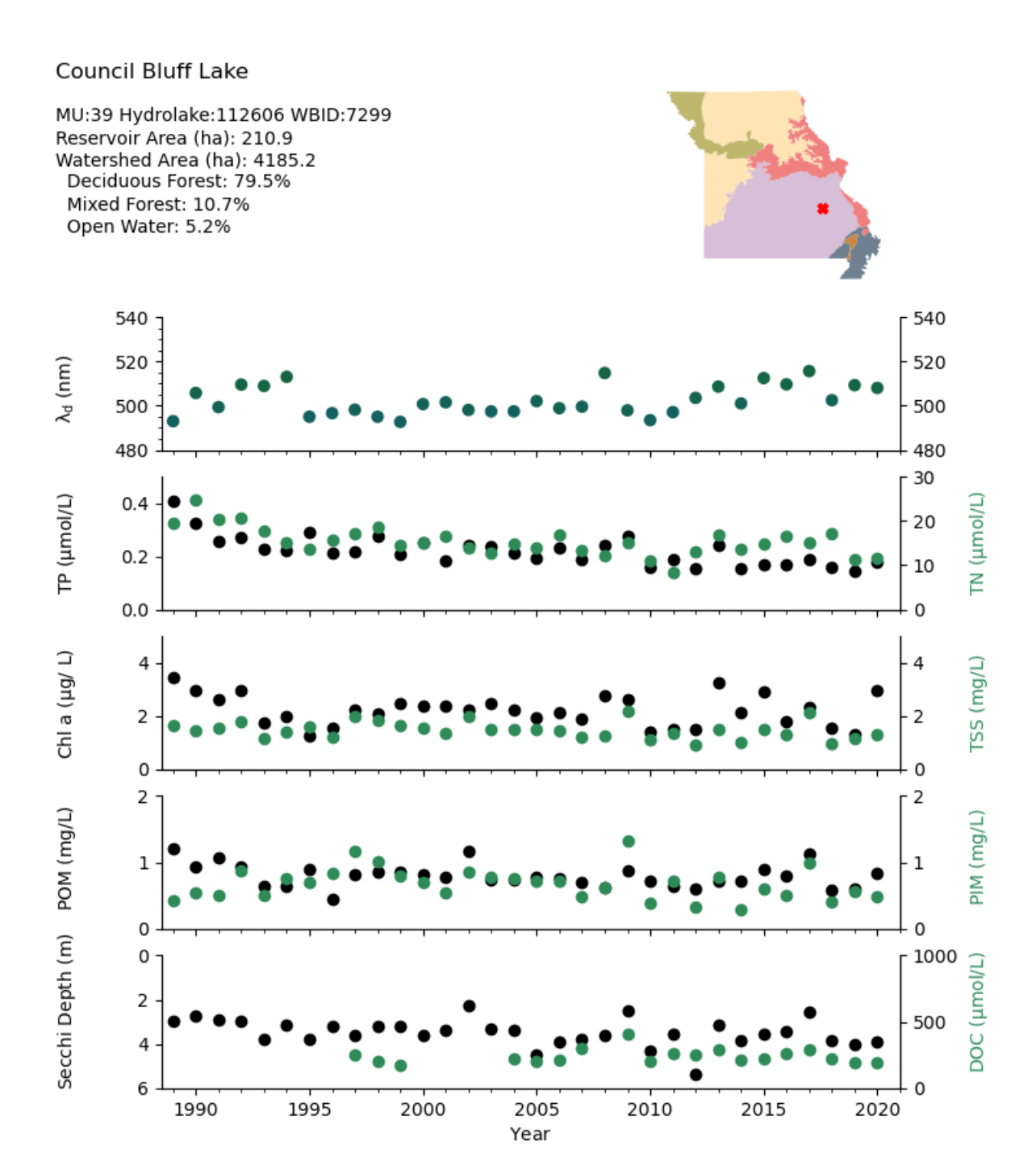


Figure S9. Water color (dominant wavelength; λ_d) and water quality (total phosphorus–TP, total nitrogen–TN, chlorophyll–Chl a, total suspended solids–TSS, particulate organic matter–POM, particulate inorganic matter–PIM, Secchi depth, and dissolved organic carbon–DOC) changes in Council Bluff Lake (Hylak_id 112606). Black and green points refer to left and right axes respectively. TP, TN, TSS and POM are significantly decreasing; λ_d and Secchi are significantly increasing.

References

Bartos, M., 2020. pysheds: Simple and fast watershed delineation in python. GitHub repository. https://github.com/mdbartos/pysheds.

Bartoń K (2024). MuMIn: Multi-Model Inference. R package version 1.48.4. https://CRAN.R-project.org/package=MuMIn.

Bates, D., Mächler, M., Bolker, B., Walker, S., 2015. Fitting linear mixed-effects models using lme4. J Stat Softw 67, 1–48.

Gillies, S., van der Wel, C., Van den Bossche, J., Taves, M.W., Arnott, J., Ward, B.C., et al., 2022. Shapely, Version 2.0.0. GitHub repository. https://github.com/shapely/shapely.

Greenwell, B., Boehmke, B., Cunningham, J., GBM Developers, 2022. gbm: Generalized Boosted Regression Models. R package version 2.1.8. https://CRAN.R-project.org/package=gbm.

Harris, C.R., Millman, K.J., van der Walt, S.J., Gommers, R., Virtanen, P., Cournapeau, D., Wieser, E., Taylor, J., Berg, S., Smith, N.J., Kern, R., Picus, M., Hoyer, S., van Kerkwijk, M.H., Brett, M., Haldane, A., del Río, J.F., Wiebe, M., Peterson, P., Gérard-Marchant, P., Sheppard, K., Reddy, T., Weckesser, W., Abbasi, H., Gohlke, C., Oliphant, T.E., 2020. Array programming with NumPy. Nature 585, 357–362.

Hijmans, R.J., Phillips, S., Leathwick, J., Elith, J., 2023. dismo: Species distribution modeling. R package version 1.3-15. https://CRAN.R-project.org/package=dismo.

Jones, J.R., Argerich, A., Obrecht, D. V, Thorpe, A.P., North, R.L., 2024a. Missouri lakes and reservoirs long-term limnological dataset, 1976-2018. Ver 2. Environmental Data Initiative (Accessed 2024-06-14).

Jones, J.R., North, R.L., Argerich, A., Thorpe, A.P., Obrecht, D. V, Price, A., Santamaria, K., Richardson, D.C., 2024b. Missouri reservoir profile data including temperature, depth, and oxygen profiles (1989-2022). Ver 2. Environmental Data Initiative (Accessed 2024-11-01).

Kendall, M.G., 1975. Rank Correlation Methods, 4th ed. Charles Griffin, London.

Kuznetsova, A., Brockhoff, P.B., Christensen, R.H.B., 2017. lmerTest package: Tests in linear mixed effects models. J Stat Softw 82, 1–26.

Laird, N.M., Ware, J.H., 1982. Random-Effects Models for Longitudinal Data. Biometrics 38, 963–974.

Lüdecke, D., Ben-Shachar, M., Patil, I., Makowski, D., 2020. Extracting, computing and exploring the parameters of statistical models using R. J Open Source Softw 5, 2445.

Mann, H.B., 1945. Nonparametric Tests Against Trend. Econometrica 13, 245–259.

Molnar, C., Bischl, B., Casalicchio, G., 2018. iml: An R package for interpretable machine learning. J Open Source Softw 3, 786.

North, R.L., Argerich, A., Obrecht, D. V, Thorpe, A.P., Richardson, D.C., 2025. Missouri reservoir water quality data from the Statewide Lake Assessment Program (SLAP), the Lakes of Missouri Volunteer Program (LMVP), and the Reservoir Observer Student Scientists (ROSS) program. Ver 1. Environmental Data Initiative (Accessed 2025-04-24).

Pohlert, T., 2020. trend: Non-parametric trend tests and change-point detection (R package version 1.1.4). https://CRAN.R-project.org/package=trend

Sen, P.K., 1968. Estimates of the regression coefficient based on Kendall's Tau. J Am Stat Assoc 63, 1379–1389.

Van den Bossche, J., Jordahl, K., Fleischmann, M., Richards, M., McBride, J., Wasserman, J., Badaracco, A.G., Snow, A.D., Ward, B., Tratner, J., Gerard, J., Perry, M., ..., Gardiner, J., 2024. geopandas/geopandas: Version 1.0.1. Zenodo.

Winslow, L., Read, J., Woolway, R., Brentrup, J., Leach, T., Zwart, J., Albers, S., Collinge, D., 2019. RLakeAnalyzer: An R package for analyzing lake data. Journal of R Package Development 10, 1–15.